



HAL
open science

Human model of IRX5 mutations reveals key role for this transcription factor in ventricular conduction

Zeina R Al Sayed, Robin Canac, Bastien Cimarosti, Carine Bonnard, Jean-Baptiste Gourraud, Hanan Hamamy, Hulya Kayserili, Aurore Girardeau, Mariam Jouni, Nicolas Jacob, et al.

► To cite this version:

Zeina R Al Sayed, Robin Canac, Bastien Cimarosti, Carine Bonnard, Jean-Baptiste Gourraud, et al.. Human model of IRX5 mutations reveals key role for this transcription factor in ventricular conduction. Cardiovascular Research, 2021, 117 (9), pp.2092-2107. 10.1093/cvr/cvaa259 . inserm-02934863v2

HAL Id: inserm-02934863

<https://inserm.hal.science/inserm-02934863v2>

Submitted on 8 Nov 2021

HAL is a multi-disciplinary open access archive for the deposit and dissemination of scientific research documents, whether they are published or not. The documents may come from teaching and research institutions in France or abroad, or from public or private research centers.

L'archive ouverte pluridisciplinaire **HAL**, est destinée au dépôt et à la diffusion de documents scientifiques de niveau recherche, publiés ou non, émanant des établissements d'enseignement et de recherche français ou étrangers, des laboratoires publics ou privés.

**Human model of *IRX5* mutations reveals key role
for this transcription factor in ventricular conduction**

Zeina R Al Sayed, PhD¹, Robin Canac, MSc¹, Bastien Cimarosti, MSc¹, Carine Bonnard, PhD², Hanan Hamamy, MD³, Hulya Kayserili, MD-PhD⁴, Aurore Girardeau, BSc¹, Mariam Jouni¹, PhD, Nicolas Jacob, MD¹, Anne Gaignerie, MSc⁵, Caroline Chariiau, BSc⁵, Laurent David, PhD⁵⁻⁷, Virginie Forest, PhD¹, Céline Marionneau, PhD¹, Gildas Loussouarn, PhD¹, Guillaume Lamirault, MD-PhD¹, Bruno Reversade, PhD^{2,4,8-10}, Kazem Zibara, PhD¹¹, Patricia Lemarchand, MD-PhD^{1,12*}, Nathalie Gaborit, PhD^{1*}

1. l'institut du thorax, INSERM, CNRS, UNIV Nantes, Nantes, France.
2. Institute of Medical Biology, A*STAR, Singapore, Singapore.
3. Department of Genetic Medicine and Development, Geneva University, Geneva 1211, Switzerland.
4. Medical Genetics Department, Koç University School of Medicine (KUSOM), Istanbul, Turkey.
5. SFR-Santé François Bonamy, INSERM, CNRS, UNIV Nantes, CHU Nantes, Nantes, France.
6. CRTI, INSERM, UNIV Nantes, Nantes, France.
7. ITUN, CHU Nantes, Nantes, France.
8. Department of Paediatrics, National, University of Singapore, Singapore, Singapore.
9. Institute of Molecular and Cellular Biology, A*STAR, Singapore, Singapore.
10. Reproductive Biology Laboratory, Amsterdam UMC, Amsterdam-Zuidoost, Netherlands.
11. ER045, Laboratory of stem cells, DSST, Biology department, Faculty of Sciences, Lebanese University, Beirut, Lebanon.
12. l'institut du thorax, CHU Nantes, Nantes, France.

Short title: Key role of *IRX5* in human ventricular conduction

Total word count: 8992

Manuscript category: Original article

Reprint requests and correspondence:

Nathalie GABORIT, PhD and Patricia Lemarchand, MD-PhD

l'institut du thorax

Inserm UMR 1087, CNRS UMR 6291

IRS-UN, 8 quai Moncoussu

44007 Nantes cedex 1, France

E-mail: nathalie.gaborit@univ-nantes.fr and patricia.lemarchand@univ-nantes.fr.

1 **Abstract**

2 **Aim:** Several inherited arrhythmic diseases have been linked to single gene mutations in cardiac
3 ion channels and interacting proteins. However, the mechanisms underlying most arrhythmias,
4 are thought to involve altered expression regulation of multiple effectors. In this study, we
5 aimed to examine the role of a transcription factor belonging to the Iroquois homeobox family,
6 *IRX5*, in cardiac electrical function.

7 **Methods and results:** Using human cardiac tissues, transcriptomic correlative analyses
8 between *IRX5* and genes involved in cardiac electrical activity showed that in human
9 ventricular compartment, *IRX5* expression strongly correlated to the expression of major actors
10 of cardiac conduction, including the sodium channel, Nav1.5, and Connexin 40 (Cx40). We
11 then generated human induced pluripotent stem cells (hiPSCs) derived from two Hamamy
12 Syndrome-affected patients carrying distinct homozygous loss-of-function mutations in *IRX5*
13 gene. Cardiomyocytes derived from these hiPSCs showed impaired cardiac gene expression
14 program, including dysregulation in the control of Nav1.5, Cx40 and Cx43 expression. In
15 accordance with the prolonged QRS interval observed in Hamamy Syndrome patients, a slower
16 ventricular action potential depolarization due to sodium current reduction was observed on
17 electrophysiological analyses performed on patient-derived cardiomyocytes, confirming the
18 functional role of *IRX5* in electrical conduction. Finally, a novel cardiac transcription factor
19 complex was identified, composed by *IRX5* and GATA4, in which *IRX5* potentiated GATA4-
20 induction of *SCN5A* expression.

21 **Conclusions:** Altogether, this work unveils a key role for *IRX5* in the regulation of human
22 ventricular depolarization and cardiac electrical conduction, providing therefore new insights
23 into our understanding of cardiac diseases.

24 **Keywords:**

25 *IRX5*, transcription factors, conduction, arrhythmia, Hamamy syndrome, human induced
26 pluripotent stem cells.

27 **Translational perspectives**

28 Inherited cardiac arrhythmias account for about 20% of sudden cardiac deaths, of which a small
29 portion are monogenic familial diseases with mutations in cardiac ion channels. However,
30 pathogeny of inherited cardiac arrhythmias is increasingly thought to result from complex
31 mechanisms involving altered expression regulation of multiple effectors. Taking advantage of
32 cardiomyocytes derived from Hamamy syndrome patients, carrying loss-of-function mutations
33 in *IRX5* transcription factor, we uncovered an important role for IRX5 in the regulation of
34 several major players of ventricular depolarization conduction and in arrhythmogenesis. Thus,
35 this study supports systematic screening for genetic variants in IRX5 in inherited cardiac
36 arrhythmias.

37 1. Introduction

38 Inherited cardiac arrhythmias account for about 20% of sudden cardiac deaths. Only a small
39 portion of these arrhythmias are monogenic familial diseases, having been successfully linked
40 to rare mutations in cardiac ion channels and related proteins [1]. However, pathogeny of
41 inherited cardiac arrhythmias is increasingly thought to be based on complex mechanisms
42 involving polygenic inheritance and/or altered expression regulation of multiple effectors [2].
43 In this context, investigating how dysfunction of transcriptional regulators participates in the
44 mechanism of these diseases is of major importance.

45 The regulation of global cardiac electrical transcriptional program, including ion channels and
46 gap junctions, is a major determinant of proper initiation and propagation of action potential
47 (AP) through the cardiac muscle. In animal models, several transcription factors (TFs) have
48 been shown to play mechanistic roles in cardiac electrical activity and arrhythmias [3,4],
49 including members of the Iroquois (IRX) family of TFs [5].

50 Autosomal recessive mutations in *IRX5*, an Iroquois homeobox TF, cause an inherited
51 congenital disorder named Hamamy Syndrome (HMMS, OMIM611174) which clinical
52 description revealed on the electrocardiogram, a QRS prolongation, illustrating a delayed
53 ventricular electrical conduction, and a bradycardia [6,7]. Surprisingly, in mice, deletion of *Irx5*
54 leads to a different phenotype, a ventricular repolarization defect, due to the role of *Irx5* in
55 controlling potassium channel gene expression [8]. Inversely, another murine member of the
56 *Irx* family, *Irx3*, is essential for fine regulation of intercellular coupling within the ventricular
57 conduction system, through the regulation of connexins expression [9,10]. This suggests that
58 distinct regulatory pathways govern the differences between human and animal cardiac
59 electrical physiology.

60 In this study, our goal was to decipher whether IRX5 controls human cardiac electrical activity.
61 First, correlative transcriptomic analyses between IRX5 and cardiac electrophysiology genes in
62 human cardiac tissues, suggested that IRX5 may regulate several major actors of cardiac
63 conduction. Then, human induced pluripotent stem cells (hiPSCs) derived from HMMS patients
64 carrying *IRX5* mutations were used to elucidate the role of IRX5 in regulating expression of
65 these actors of cardiac conduction and to uncover a cooperative activity between TFs. This
66 work reveals how LOF mutation in one key TF affects the expression of multiple effectors of
67 ventricular electrical conduction and improves our understanding of cardiac disease, paving the
68 way therefore for more effective therapies.

69 **2. Methods**

70 **Ethical Statement:**

71 The study was conducted according to the principles set forth under the Declaration of Helsinki
72 (1989) and European guidelines for clinical and genetic research. Institutional review board
73 approvals of the study were obtained before the initiation of patient enrollment. Regarding the
74 patient-derived biological samples, signed informed consent allowing the experiments to be
75 conducted have been received from all individuals. Any related health information was
76 collected in compliance with applicable law/regulation and with any applicable policy of the
77 ethics committee with jurisdiction over the biological sample collection. All biological samples
78 and their related health information have been provided in coded form such that subjects cannot
79 be identified directly. The provisions of French law, article L1110-4 of the Code de la santé
80 publique, related to the privacy and confidentiality of information regarding patients, have been
81 observed. The transfer of the Hamamy syndrome-affected (HMMS) patient's biological
82 samples has complied with all applicable laws as well as legal, regulatory and ethical
83 requirements in transferring and obtaining such Material and the corresponding informed
84 consents (Authorization IE 2009-505(1)).

85 **2.1 Transcriptional analysis of human and murine tissues**

86 RNA sequencing data in human heart were collected from the GTEx portal website
87 (<http://gtexportal.org>). Briefly, transcripts per million (TPM) were downloaded for 297 atrial
88 and 303 ventricular available tissue samples.

89 Regarding murine samples, animal experiments were performed in accordance with
90 institutional guidelines for animal use in research. Hearts were excised from six 10-week-old
91 C57BL/6 male mice and atria and ventricles were carefully dissected as previously described
92 [11].

93 Two-way hierarchical agglomerative clustering was applied to gene-expression matrices (see
94 TLDA section below), by centering gene expression values on the values-median and using
95 average linkage-clustering with uncentered correlation (Cluster 3.0). GTEx left ventricular
96 tissues RNA sequencing data of major cardiac sodium channels and connexins were ranked
97 according to ascending expression of IRX5. Expression correlations were tested using Pearson
98 correlation package on R software.

99 **2.2 Human induced pluripotent stem cells (hiPSC) generation**

100 Primary dermal fibroblasts were derived from skin biopsies were obtained from donors of two
101 different consanguineous families, previously described with Hamamy Syndrome [6,7]. The
102 first diseased donor is a 4-year-old boy, homozygous carrier of the c.448G>C *IRX5* mutation
103 (p.Ala150Pro annotated as A150P) in whom a QRS prolongation on the ECG was diagnosed.
104 The second donor is a 17-year-old boy belonging to another family harboring the homozygous
105 c.498C>A *IRX5* mutation (p.Asn166Lys annotated as N166K) who presents a prolonged QRS
106 duration on the ECG, in addition to a tiny patent ductus arteriosus. In parallel, fibroblasts from
107 three individuals lacking the *IRX5* mutations were used as controls: the unaffected sister of the
108 first donor, a healthy subject with comparable gender, age, and ethnicity as second donor, as
109 well as an unrelated previously described control [13]. HiPSC lines were generated using
110 Sendai virus method. For each line, two to three hiPSC clones were selected and expanded on
111 stem cell-qualified Matrigel-coated plates (0.1 mg/ml; BD Bioscience) with StemMACS™ iPS
112 Brew XF medium (Miltenyi Biotec).

113 **2.3 HiPSC characterization**

114 For all clones, genomic DNA was extracted and mutations were verified by sequencing using
115 primers specific for the genomic regions surrounding the A150P and N166K mutations
116 (Supplemental Table 1). Pluripotency marker gene expression was assessed using flow
117 cytometry, qRT-PCR, and immunofluorescence as previously described [13]. Single nucleotide
118 polymorphism (SNP) analysis of hiPSCs compared to their parental skin fibroblast cells was
119 used to confirm genome integrity after reprogramming. DNA was extracted from somatic and
120 hiPSC samples using the QIAGEN QiaAmp kit, according to the manufacturer's
121 recommendations. The gDNA was quantified using a nanodrop. 200 ng of gDNA was
122 outsourced to Integragen Company (Evry, France) for karyotype analysis using HumanCore-
123 24-v1 SNP arrays. This array contains over 300,000 probes distributed throughout the genome
124 with a median coverage of one probe every 5700 bases. All genomic positions were based on
125 Human Genome Build 37 (hg19). Analysis was performed with GenomeStudio software.
126 Chromosome abnormalities were determined by visual inspection of logR ratios and B-allele
127 frequencies (BAF) values and comparing parental cells and hiPS-derived samples. LogR ratio,
128 the ratio between observed and expected probe intensity, is informative of copy number
129 variation (CNV, *i.e.*, deletions/duplications), whereas BAF is informative of heterozygosity.
130 SNP data was used to compute CNV. In particular, this type of chips allows detecting loss of
131 heterozygosity (LOH), an important concern for hiPSC, which is not detectable with classical
132 CGH arrays.

133 **2.4 Differentiation of hiPSCs into cardiomyocytes (CMs)**

134 At 80% of cell confluency, hiPSC lines were passaged using Gentle Cell Dissociation Reagent
135 (STEMCELL Technologies) and Y-27632 Rho-kinase inhibitor (STEMCELL Technologies).
136 The matrix sandwich method was used to generate CMs, as previously described [13]. From
137 day 5 of differentiation, cell media was changed every other day with RPMI-1640 medium
138 supplemented with B27 (with insulin; Thermo Fisher Scientific). After 20 to 28 days following
139 the beginning of differentiation, spontaneously beating cell clusters were mechanically isolated
140 using a needle and then used for electrophysiological, biochemical and molecular analyses.

141 **2.5 RNA expression**

142 **RNA extraction:** Samples of total RNA were obtained using the NucleoSpin RNA kit
143 (MACHEREY-NAGEL) following manufacturer's specifications.

144 **TaqMan low-density array (TLDA) :** TLDA studies were conducted using six ventricular and
145 six atrial control murine tissues as well as beating clusters of hiPS-CMs obtained from 12
146 control and 9 *IRX5*-mutant CM differentiations. 1 μ g of RNA was reverse transcribed into
147 cDNA using SuperScript IV Vilo Master Mix (Thermo Fisher Scientific). For murine tissues,
148 three specifically designed 384-well TLDA were used: one containing 4x 96 primers and probes
149 for cardiac ion channels [11] and 2 others, each containing a set of 4x 96 primers and probes
150 for cardiac transcription factors (Supplemental Table 2A). For hiPS-CMs, TLDA probe
151 selection covered gene families implicated in cardiac ion channel expression and regulation,
152 and cardiomyocyte structure (Supplemental Table 2B). Genes with average Ct > 32 in all
153 compared groups were considered undetectable and excluded from the analysis (*SCN10A* and
154 *ABCC8*). Average Ct of remaining genes for each sample was used for data normalization [14–
155 16].

156 **3' Sequencing RNA Profiling (3'SRP):** 3'SRP protocol was performed according to Kilens
157 et al [17]. Briefly, the libraries were prepared from 10 ng of total RNA. 40 RNA samples were
158 extracted from 8 *IRX5*-mutated and 13 control hiPSC samples (a duplicate for each clone
159 obtained at different cell passages) and 19 samples of corresponding hiPS-CMs. The mRNA
160 poly(A) tail was tagged with universal adapters, well-specific barcodes and unique molecular
161 identifiers (UMIs) during template-switching reverse transcriptase. Barcoded cDNAs from
162 multiple samples were then pooled, amplified and tagged using a transposon-fragmentation
163 approach which enriches for 3'ends of cDNA. A library of 350-800bp was run on an Illumina
164 HiSeq 2500 using a HiSeq Rapid SBS Kit v2 (50 cycles; FC-402-4022) and a HiSeq Rapid PE
165 Cluster Kit v2 (PE-402-4002). Read pairs used for analysis matched the following criteria: all

166 sixteen bases of the first read had quality scores of at least 10 and the first six bases correspond
167 exactly to a designed well-specific barcode. The second reads were aligned to RefSeq human
168 mRNA sequences (hg19) using bwa version 0.7.4 4. Reads mapping to several positions into
169 the genome were filtered out from the analysis. Digital gene expression profiles were generated
170 by counting the number of unique UMIs associated with each RefSeq genes, for each sample.
171 R package DESeq2 was used to normalize gene expression. Differentially expressed genes were
172 finally clustered using cluster 3.0 software. Enriched biological pathways were assigned for
173 differentially expressed genes in *IRX5*-mutated vs. control hiPS-CMs. For that, Reactome
174 pathways were attributed to the most variant genes with p-value <0.05 [18,19]. However, genes
175 encoding for ion channels exhibited low expression levels and therefore they were not taken
176 into consideration for differentially expressed genes analysis. To overcome this issue, p-values
177 for these genes were calculated based on TLDA analysis. Babelomics was then used to calculate
178 enrichment of Reactome pathways for genes differentially expressed in both TLDA and 3'SRP
179 analyses. Finally, enrichment scores (ES) were calculated [20,21].

180 **2.6 Protein expression and interaction**

181 **Protein extraction:** *IRX5*, *Nav1.5*, *Cx40* and *GATA4* expression were evaluated in human left
182 and right ventricular tissues obtained from three non-diseased individuals as previously
183 described [22]. Corresponding sub-endocardial and sub-epicardial tissue slices were obtained
184 at the cardiac base and snap-frozen in liquid nitrogen. Protein expressions and interactions were
185 also investigated in beating hiPS-CMs at day 28 of differentiation. For protein extraction, cells
186 were homogenized on ice using lysis buffer containing in mM: 1% TritonX-100; 100 NaCl; 50
187 Tris-HCl; 1 EGTA; 1 Na₃VO₄; 50 NaF; 1 phenylmethylsulfonyl fluoride and protease inhibitors
188 cocktail (P8340, Sigma-Aldrich). Extracted samples were sonicated and centrifuged at 15,000
189 × g for 15 min at 4°C. Protein quantification was carried out using Pierce™ BCA Protein Assay
190 Kit (Thermo Fisher).

191 **Subcellular protein fractionation:** To unveil the impact of *IRX5* mutations on its cellular
192 localization, nuclear and cytosolic proteins were separated. For that, cytoplasmic membranes
193 were disrupted on ice in a hypotonic solution including in mM: 500 HEPES, 500 MgCl₂, 500
194 KCl, 0.1 DTT and protease inhibitor cocktail. Cells nuclei were pelleted by 2000 rpm
195 centrifugation and the supernatant contained the cytosolic fraction. In order to extract nuclear
196 proteins, a protein extraction buffer was added to pellets followed by sonication.

197 **Co-immunoprecipitation:** This was performed to investigate protein-to-protein interactions
198 between *IRX5* and *GATA4* in hiPS-CMs. A total of 12.5 μl magnetic Dynabeads® Protein G

199 (Thermo Fisher Scientific) were added to 3 µg anti-IRX5 antibody (WH0010265M1, Sigma-
200 Aldrich) or anti-mouse IgG antibody as control (02-6502, Thermo Fisher Scientific) and
201 conjugated by incubation for 40 min at room temperature with rotation. The complex beads-
202 antibody was cross-linked using 27 mg DMP (dimethyl pimelimidate, Thermo Fisher
203 Scientific), and then incubated for 2 hours with 800 µg of total lysate at 4°C. The supernatant
204 was then discarded and the beads were washed with the lysis buffer. Proteins were eluted in 30
205 µl of a mixture of NuPAGE® Sample Reducing Agent (10X) and LDS Sample Buffer (4X)
206 (Invitrogen) and heated at 60°C. The samples were then loaded onto a 4-15% precast
207 polyacrylamide gel (Bio-Rad).

208 **2.7 Immunofluorescence**

209 HiPSCs or hiPS-CMs at day 20 of differentiation were dissociated using collagenase II (Gibco)
210 and seeded onto 8-wells iBidi plates (Biovalley) coated with Matrigel (Corning). Twelve days
211 later, cultured cells were immunostained using a staining buffer set according to the
212 manufacturer's instructions (00-5523-00, Thermo Fisher Scientific). HiPS-CMs were labeled
213 by cardiac differentiation markers, *i.e.*, Troponin I (Santa Cruz) and Troponin T (Abcam)
214 together with either cardiac conduction actors, *i.e.*, Nav1.5 (Cell signaling), Cx40 (Santa Cruz)
215 and Cx43 (Sigma) or transcription factor, *i.e.*, IRX5 (Sigma-Aldrich). DNA was highlighted
216 using DAPI and pictures were taken using confocal microscopy (Nikon; MicroPICell core
217 facility).

218 **2.8 Chromatin immunoprecipitation (ChIP)**

219 **IRX5 binding sites:** Promoter DNA sequences were found using Ensembl. Consensus
220 sequences known to mediate Iroquois transcription factor interaction with DNA [23–25] were
221 screened on gene promoters. Each site was verified for its conservation among species using
222 rVista 2.0. Primers surrounding the identified conserved potential binding sites (BS) were
223 designed using Primer 3. Corresponding primer sequences are detailed in Supplemental Table
224 3.

225 **ChIP:** At day 28 of differentiation, beating cardiomyocyte clusters were isolated and
226 crosslinked. After chromatin sonication, IRX5 antibody was added followed by the addition of
227 protein G-coated dynabeads. Following an overnight incubation, the chromatin was then eluted
228 and reverse-crosslinked. SYBER green qRT-PCR method was finally performed using the
229 designed primers (Supplemental Table 3) to test for enrichment of the targeted sequences.
230 Results are shown as percentage of input.

231 **2.9 Cellular electrophysiology**

232 **Cell dissociation:** hiPS-CMS were enzymatically dissociated into single cells using
233 collagenase II (Gibco) at 37°C for 20 min. Cells were then incubated at RT for 30 min in Kraft-
234 Bruhe solution containing (in mM): 85 KCl; 30 K₂HPO₄; 5 MgSO₄; 20 glucose; 20 taurine; 5
235 Na pyruvate; 5 creatine; 2 K₂-ATP; 1 EGTA; pH 7.2 adjusted with KOH. Single cells were
236 then plated at low density on Matrigel-coated Petri-dishes (Nunc) and recorded 11 to 14 days
237 after dissociation.

238 **Data recording and analysis:** Stimulation and data recording were performed at 37°C using
239 an Axopatch 200B amplifier controlled by Axon pClamp 10.6 software through an A/D
240 converter (Digidata 1440A) (all Molecular Devices). Data were analyzed using Clampfit 10.6
241 software. For all cell lines, data were collected from at least 3 independent differentiations.
242 Experimental details regarding solutions composition are described in Supplemental Table 4.

243 **Current clamp:** Action potential (AP) recordings were obtained using the amphotericin-B-
244 perforated patch-clamp technique. Patch pipettes were pulled from borosilicate glass capillaries
245 (Sutter instruments) to obtain a tip resistance of 2 to 3 MΩ were utilized. APs were first
246 recorded from spontaneously beating cells which were then paced by injecting a current density
247 of 30-35 pA/pF during 1 ms, at various frequencies. Based on several parameters previously
248 described (maximum upstroke velocity, dV/dt_{max} ; action potential duration, APD; resting
249 membrane potential, RMP), cells were classified as either ventricular, atrial or nodal [12]. Only
250 ventricular cells were selected for further analysis. Electronic expression of the inward rectifier
251 potassium current, I_{K1} , was realized using dynamic patch-clamp [26]. At 2 pA/pF of *in silico* I_{K1}
252 injection, hiPS-CM membrane resting potential was about -80 ± 10 mV. Averaged parameters
253 were obtained from 7 consecutive APs. Both cell stimulation and injection of I_{K1} were realized
254 by a custom-made software running on RT-Linux and a National Instrument A/D converter (NI
255 PCI-6221) connected to the current command of the amplifier.

256 **Voltage clamp:** I_{Na} and $I_{Ca,L}$ recordings were performed in the ruptured whole-cell
257 configuration using voltage clamp protocol as depicted in the figures. Pipettes (Sutter
258 instruments) with 1.7-2.5MΩ tip resistance were waxed before use to decrease pipette capacitive
259 currents. $I_{Ca,L}$, and I_{Na} recordings were low-pass filtered at, respectively, 3 KHz and 10 KHz.
260 Holding potentials were respectively -80 mV and -100 mV. The capacitance and series were
261 compensated using a VE-2 amplifier (Alembic Instrument, Qc, Canada). Leak current was
262 subtracted. Current densities were calculated by dividing the current to the membrane
263 capacitance (C_m). Steady-state activation and inactivation curves were fitted using a Boltzmann

264 equation: $I/I_{max} = A / \{1.0 + \exp [(V_{1/2} - V)/k]\}$ with $k > 0$ for the activation curve and $k < 0$ for the
265 inactivation curve.

266 **Action potential clamp:** In order to record specific currents during AP cycles, and especially
267 during the depolarization phase, cells membrane potential was clamped according to voltage-
268 AP-like protocols. Representative APs acquired from spontaneously beating control hiPS-CMs
269 with ($dV/dt_{max} = 100$ V/s; $APD_{90} = 280$ ms; $RMP = -83$ mV) or without ($dV/dt_{max} = 12$ V/s;
270 $APD_{90} = 300$ ms; $RMP = -57$ mV) *in silico* I_{K1} injection were selected. Activated sodium current
271 during AP was measured by subtracting traces before and after adding $30 \mu\text{M}$ tetrodotoxin TTX
272 in I_{Na} -specific intracellular and extracellular (with 130 mM NaCl concentration) solutions
273 (Supplemental Table 4). $I_{Ca,L}$ was considered as the Nifedipine-sensitive ($4 \mu\text{M}$) calcium
274 current recorded using $I_{Ca,L}$ solutions (Supplemental Table 4).

275 **2.10 Luciferase assay**

276 *SCN5A* BS2- (from -261 to $+613$ bp of the TSS) and BS2+ (from -261 to $+1072$ bp from TSS)
277 Plasmids (150 ng), pGL2-Renilla (15 ng) with or without GATA4 expressing vector (150 ng)
278 and with or without either of the wild-type or mutated forms of *IRX5* expressing vectors (150
279 ng) were transfected into HEK293 cells using Lipofectamine 2000 (Thermo Fisher Scientific).
280 DNA quantities were equalized in each condition using empty pcDNA3.1. Cells were harvested
281 48 hours later and luciferase activity was measured using Dual Luciferase reporter assay system
282 (Promega).

283 **2.11 Microscale Thermophoresis (MST)**

284 MST was used to verify protein interaction with DNA according to Nanotemper instructions.
285 Briefly, HEK293 cells transfected by *IRX5-GFP* expressing vector were used to produce
286 fluorescently labeled *IRX5* protein. Cell lysates were prepared using a buffer containing 20 mM
287 Tris HCl, 130 mM NaCl, 1% NP40 and protease inhibitors cocktail. Titration series were
288 performed to obtain varying concentrations of *SCN5A* plasmids. Measurements were
289 accomplished in standard treated capillaries on Monolith NT.115 instrument using 80% of laser
290 power.

291 **2.12 Statistical analysis**

292 Results are expressed as mean \pm SEM. Comparisons were made by use Student *t*-test, or two-
293 way ANOVA with Bonferroni post-hoc test for repeated measures. Values of $p < 0.05$ were
294 considered statistically significant. Statistical analyses were performed with GraphPad Prism
295 software.

296 **3. Results**

297 **3.1 IRX5 TF expression correlates with conduction genes expression in human cardiac**
298 **tissues**

299 In order to identify evolutionary-conserved *IRX5*-coregulated genes in contractile tissues,
300 expression profiles of cardiac genes including ion channels and TFs were compared between
301 murine and human tissues. Overall, the global gene expression contrast profile between atrial
302 and ventricular murine tissues were conserved in human samples (Figure 1A). The cluster of
303 genes that are more expressed in ventricular tissues, included *IRX5* and several genes involved
304 in cardiac conduction, such as *SCN5A*, which encodes the main cardiac sodium channel $Na_v1.5$
305 (Figure 1A). Then, the correlations between *IRX5* gene expression level and those of sodium
306 channels and connexins (Cx), the two main families of genes implicated in cardiac conduction
307 in humans, were investigated in the ventricles. Interestingly, *SCN5A* and *GJA5*, encoding one
308 of the main cardiac Cx, Cx40, showed the strongest correlations with *IRX5* (Figure 1B). In
309 accordance with these results and confirming previous results concerning *IRX5* human protein
310 expression [22], both $Na_v1.5$ and Cx40 shared a gradient of protein expression similar to that
311 of *IRX5* throughout the human ventricular wall with a higher level in sub-endocardium as
312 compared to sub-epicardium (Figure 1C).

313 Taken together, these analyses shed light on the importance of studying the role of *IRX5* in the
314 regulation of cardiac ventricular genes, and more specifically in the regulation of players of
315 cardiac electrical conduction in human ventricles. The analysis of the role of *IRX5* in humans
316 was then pursued using hiPSCs obtained from three non-diseased individuals (shown as
317 averaged) as well as from two patients carrying different loss-of-function (LOF) mutations in
318 *IRX5* gene associated to a QRS prolongation on the ECG (Figure S1A) [7].

319 **3.2 IRX5-mutated hiPS-CMs derived from HMMS patients are a relevant model to study**
320 **IRX5 role.**

321 Dermal fibroblasts of two homozygous carriers of either the A150P- or the N166K-*IRX5*
322 mutation [7] and of 3 intra- and extra-familial control subjects were reprogrammed into hiPSCs.
323 Mutations were confirmed by sequencing in hiPSCs (Figure S1B). Genome integrity was
324 validated using SNP analysis (data not shown). Expression of pluripotency markers was
325 verified in hiPSCs (Figure S1C-E).

326 We then investigated whether all hiPSC lines differentiated in a comparable manner. Principal
327 Component Analysis (PCA) of individual transcriptomic profiles as well as correlation analysis

328 showed that samples mainly clustered according to their differentiation stage (Figure 2A and
329 2B). Furthermore, all control and *IRX5*-mutated hiPS-CMs presented a similar global change
330 in gene expression compared to that of hiPSCs (Figure 2C). These data showed that all hiPSCs,
331 irrespectively of their genetic background, differentiated similarly into cardiac cells.
332 Immunostaining analysis showed that striated Troponin I was present in CMs derived from each
333 hiPSC line (Figure 2D). Moreover, the proportions of nodal-like, atrial-like and ventricular-like
334 cells identified using patch-clamp were comparable in control and mutated hiPS-CMs, with the
335 ventricular-like type forming the majority of hiPS-CMs (Figure 2E). Altogether, these data
336 confirmed that control and *IRX5*-mutated hiPSCs differentiated similarly into cardiomyocytes,
337 and therefore that hiPS-CMs are a relevant model to investigate the role of *IRX5* in ventricular
338 electrical conduction.

339 Regarding the impact of *IRX5* mutations on its own expression, transcriptional analysis and
340 nuclear protein expression revelation showed comparable *IRX5* expression levels in control
341 and *IRX5*-mutated hiPS-CMs (Figure 2F-2G). Finally, immunostainings of hiPS-CMs
342 constantly showed localization of *IRX5* in CM nuclei (Figure 2D). These data showed that
343 A150P and N166K mutations neither alter *IRX5* expression nor its localization in hiPS-CMs.

344 **3.3 Key cardiac electrical conduction gene expression depends on *IRX5***

345 Global transcriptomic analysis in hiPS-CMs, using 3'SRP, unveiled 745 genes differentially
346 expressed between control and *IRX5*-mutated cells, including several cardiac electrical
347 conduction genes (Figure 3A). Using high-throughput real-time RT-PCR (TLDA) we also
348 analyzed a set of 96 genes, including mostly genes with low expression level that could not be
349 properly detected using 3'SRP (Figure 3B). Overall, for the genes detected with both
350 techniques, expression profiles were concordant (Figure S2). Biological pathway enrichment
351 analysis revealed that differentially expressed genes were enriched in muscle contraction
352 pathway, and more specifically in the cardiac conduction and phase 0 AP-depolarization
353 functions, mainly linked to the activity of *SCN5A* and *GJA5* (Figure 3C). More precisely,
354 analyses of *IRX5*-A150P and -N166K hiPS-CMs concordantly showed major mRNA and
355 protein expression reductions of both *SCN5A* and *GJA5* (Figure 4A-4B). Also, confocal
356 microscopy further confirmed that $\text{Na}_v1.5$ and Cx40 expression was decreased in troponin T
357 positive *IRX5*-A150P and -N166K mutated hiPS-CMs (Figure 4C). In accordance with the
358 delayed conduction in HMMS patients, mRNA and protein levels of Cx43, which has a lower
359 conductance than Cx40, were increased in both mutated hiPS-CMs, with an apparent

360 abnormally cytoplasmic localization, suggesting that this increase in Cx pool may not be
361 functional (Figure S3).

362 Taken together, hiPS-CMs carrying *IRX5* LOF mutations, exhibited altered expression of key
363 genes involved in cardiac electrical conduction, suggesting a role for *IRX5* in the direct
364 transcriptional control of these genes.

365 **3.4 AP depolarization and I_{Na} density are modulated by *IRX5***

366 Given the delayed ventricular conduction phenotype observed in HMMS, a slower AP
367 depolarization in patient-derived hiPS-CMs was expected. However, the depolarization
368 velocity (dV/dt_{max}) of ventricular APs, was not statistically reduced in *IRX5*-mutated hiPS-CMs
369 (Figure 5A). Therefore, we hypothesized that this could be due to low I_{K1} density, as recorded
370 cellular resting membrane potentials (RMPs) of all hiPS-CMs were at about -60mV (Figure
371 5B), that may not be suitable for proper activation of depolarizing currents. To overcome this
372 issue, an *in-silico* I_{K1} injection was performed. It brought ventricular RMPs to about -80mV
373 (Figure 5B) and revealed a significant reduction in dV/dt_{max} in *IRX5*-mutated hiPS-CMs (Figure
374 5C). The contribution of I_{Na} and $I_{Ca,L}$ to AP depolarization was then investigated. They were
375 measured when ventricular-like AP voltages, recorded with or without I_{K1} injection, were
376 applied to control hiPS-CMs. Without I_{K1} injection, $I_{Ca,L}$ contribution to the depolarization
377 phase was greater than that of I_{Na} , while with I_{K1} injection, I_{Na} became the main contributor
378 (Figure 5D). This suggests that the dV/dt_{max} reduction observed in *IRX5*-mutated hiPS-CMs
379 under I_{K1} injection was due to a functional reduction of I_{Na} , but not of $I_{Ca,L}$. Confirming this
380 hypothesis, I_{Na} was reduced by half in *IRX5*-mutated hiPS-CMs (Figure 5E and Figure S4A)
381 without any change in the (in)activation kinetics (Figure S4B and Supplemental Table 5). In
382 contrast to I_{Na} reduction, no modification in $I_{Ca,L}$ density was observed (Figure 5F). Together
383 with the *SCN5A* expression alteration, these data suggest that a slower ventricular AP
384 depolarization due to I_{Na} reduction may participate to the prolonged QRS observed in HMMS.

385 **3.5 *IRX5* interacts with *SCN5A*, *GJA5* and *GJA1* promoters**

386 Considering the altered transcription of *Cx* and *SCN5A* induced by *IRX5* LOF, we explored
387 whether *IRX5* regulates directly their promoters. An *in-silico* analysis showed that *SCN5A*
388 promoter region includes three potential TF-binding sites (BS) for *IRX5* (Figure 6A). In
389 accordance with previous studies on mice [9], human *GJA5* promoter region was free from any
390 conserved *IRX* BS (Figure 6B) while *GJA1* promoter contained 2 conserved *IRX* BSs (Figure
391 6C). Immunoprecipitation of *IRX5*-associated chromatin showed an enrichment of *SCN5A*-BS2

392 in control hiPS-CMs, revealing an interaction with IRX5, but not in *IRX5*-mutated hiPS-CMs
393 (Figure 6A). On the other hand, despite the absence of *in-silico* identification of conserved *IRX*-
394 *BS* on *GJA5* promoter, an interaction between IRX5 and *GJA5* core promoter was found in
395 control hiPS-CMs, that was again absent in *IRX5*-mutated hiPS-CMs (Figure 6B). Finally,
396 binding of IRX5 was detected on *GJAI-BS1* in control hiPS-CMs that was again not observed
397 in *IRX5*-mutated iPS-CMs (Figure 6C). These data strongly suggest that IRX5 interacts with
398 *SCN5A*, *GJA5*, and *GJAI* promoters to regulate their expression in hiPS-CMs.

399 To further investigate the direct interaction between *SCN5A* promoter and IRX5, their binding
400 affinity was evaluated. Two different DNA constructs containing *SCN5A* promoter were used:
401 BS2+ plasmid, containing *IRX5 BS2* and BS2- plasmid, lacking *IRX5 BS2*. Interestingly, IRX5
402 protein did bind to BS2+ plasmid but not to BS2- plasmid, confirming that IRX5 protein binds
403 to *SCN5A* promoter when BS2 is present (Figure 6D).

404 Finally, the functional consequences of IRX5 binding on *SCN5A* promoter were further
405 evaluated using luciferase assay with the BS2+ plasmid construct. Unexpectedly, neither IRX5
406 nor its mutated forms activated the *luciferase* reporter gene (Figure 6E), indicating that another
407 TF may be required to allow IRX5 to regulate *SCN5A* expression. This prompted us to
408 investigate the role of potential critical partners for IRX5, already known to be important for
409 regulation of cardiac development and electrical function, such as GATA4. GATA4, a
410 cardiogenic TF, has indeed been previously shown to regulate *SCN5A* expression [27] and an
411 interaction between *Irx5* and another member of the Gata family of TFs, *Gata3*, has been
412 unveiled during craniofacial development [7].

413 **3.6 IRX5 and GATA4 cooperatively regulate *SCN5A* expression in human cardiomyocytes**

414 Comparably in human cardiac ventricular samples and control hiPS-CMs, among GATA family
415 members, GATA4 was the most strongly expressed (Figure 7A). In control hiPS-CMs, GATA4
416 co-immunoprecipitated with IRX5 and this interaction was not altered in *IRX5*-mutated hiPS-
417 CMs (Figure 7B). As *SCN5A* promoter contains two sites for GATA4 binding (*BSa* and *BSb*)
418 [27], ChIP experiments using IRX5 antibody showed that IRX5 interacted with *GATA4 BSb*
419 region in control and *IRX5*-mutated hiPS-CMs (Figure 7C). Binding affinity analysis further
420 validated the direct interaction between *SCN5A* promoter and the heterodimer IRX5-GATA4,
421 as a binding was observed when both IRX5 and GATA4 proteins were mixed with BS2-
422 plasmid, in opposition to when IRX5 alone was mixed with BS2- plasmid (Figure S5).
423 Therefore, IRX5 not only binds directly to *BS2* on *SCN5A* promoter but also binds the *BSb* site
424 together with GATA4. Finally, to further dissect the role of IRX5 and GATA4 on *SCN5A*

425 transcription activation, luciferase assays were performed with plasmids containing either *BSb*
426 only (BS2- plasmid) or *BSb* and *BS2* (BS2+ plasmid). Co-transfection of GATA4 expressing
427 vector with either plasmid triggered a similar increase in luciferase activity, confirming that
428 GATA4 activated *SCN5A* promoter through a direct interaction with *BSb* (Figure 7D).
429 Interestingly, when IRX5 was added to these combinations, it potentiated by 1.6 times the effect
430 of GATA4 on BS2- plasmid, and by 3.9 times the effect of GATA4 on BS2+ plasmid (Figure
431 7D). This further demonstrated that the direct binding of IRX5 to *BS2* is important for proper
432 activation of *SCN5A* expression. Conversely, no potentiation of GATA4 activation of *SCN5A*
433 promoter was observed when A150P- or N166K-mutated IRX5 were added to the various
434 combinations (Figure 7D). Interestingly, in contrast to *IRX5* and *SCN5A*, which shared
435 similarly-graded expression patterns, *GATA4* was homogeneously expressed both in atria and
436 ventricles, and throughout the ventricular wall (Figure S6A-D). This suggests that GATA4
437 triggers basal expression of *SCN5A* throughout cardiac tissues, while IRX5 is responsible for
438 the establishment of its expression gradient.

439 **4. Discussion**

440 This study demonstrates that IRX5 TF is instrumental for proper control of electrical activity
441 in human cardiomyocytes. Overall, the present data suggest that the specific ventricular
442 transmural expression pattern of IRX5 is essential for graded regulation of sodium channel- and
443 connexin-gene expression, ensuring coordinated conduction of the electrical influx through the
444 ventricles.

445 **4.1 HiPSCs as a model to study TFs**

446 It is commonly acknowledged that stem cell-derived cardiomyocytes fail to recapitulate adult
447 CM features [28]. Nevertheless, hiPS-CMs have been used successfully so far in more than 35
448 studies of cardiac arrhythmic diseases and channelopathies [28]. Recently, 2 studies showed
449 the role of TFs in cellular dysfunction associated to cardiac morphogenetic and electrical
450 defects using hiPS-CMs [29,30]. The present work additionally enforces the use of hiPSCs as
451 a relevant model for studying the role of TF in the regulation of cardiac electrical conduction.
452 Indeed, with *in-silico* I_{K1} injection, we revealed cellular phenotypic traits that are consistent
453 with the patient's clinical phenotype, *e.g.* QRS complex prolongation observed on the patient's
454 ECG.

455 **4.2 Interspecies regulatory pathway differences**

456 Electrophysiological properties across species are known to be different [31], suggesting that
457 the roles of cardiac TFs can differ from one species to another. Here, in agreement with this
458 postulate, comparably to what was previously demonstrated for *Irx3* and its regulation of fast
459 conduction in the murine heart [9], a direct repression of *GJA1* and indirect induction of *GJA5*
460 by IRX5 has been described in human iPS-derived cardiomyocytes. However, *Irx5*KO mice did
461 not exhibit conduction delay and murine *Irx5* was not found to regulate the expression of *Cx*
462 [32].

463 Moreover, the patients, unlike *Irx5*KO mice, do not display ventricular repolarization
464 abnormalities, but a conduction defect. Indeed, the deletion of *Irx5* in mice leads to the
465 abolishment of the T wave on the ECG due to the loss of the transmural gradient of expression
466 of *Kcnd2*, at the root of one major player of ventricular repolarization in mice, I_{to}, but not in
467 human heart, where *KCND3* constitute the predominant alpha-subunit generating I_{to} [22].
468 Another argument in favor of interspecies differences in gene regulation by IRX TFs is that,
469 due to its transmural gradient of expression, *Irx5* establishes gradients of expression for its
470 target genes. That is how, in mice, *Kcnd2* ventricular gradient is known to be established. In

471 human, it is unlikely that IRX5 regulates *KCND3* expression, as, in opposition to IRX5, its
472 expression is uniform across the ventricular wall [8,22].

473 Along with this rationale, in this study, using patient-derived cardiomyocytes, a role for IRX5 in
474 the regulation of the expression of the major actors of conduction of the electrical influx, sodium
475 channel subunit and connexins, was elucidated. These data illustrate interspecies differences in
476 the mechanism of action of Iroquois TFs, demonstrating the importance of using appropriate
477 models to study human diseases.

478 **4.3 Complex regulatory pathway underlies electrical conduction**

479 Conduction of electrical influx throughout the ventricles is mediated not only by connexins but
480 also by inward currents responsible for the depolarization phase of APs. Here, among these
481 inward currents (I_{Na} and $I_{Ca,L}$), I_{Na} reduction has been identified as the trigger of the impaired
482 AP upstroke velocity in mutated hiPS-CMs. In agreement, IRX5 binds to and activates *SCN5A*
483 proximal promoter in control hiPS-CMs whereas mutations in IRX5 prevent this interaction.
484 Surprisingly, at the functional level, luciferase assays showed that IRX5 alone was not able to
485 activate *SCN5A*, suggesting that regulation of *SCN5A* is due to a combinatorial effect of several
486 factors. In accordance, IRX5 and GATA4 have been found to interact with each other allowing
487 IRX5 to bind to a previously described *GATA4 BS* on *SCN5A* promoter and to enhance GATA4
488 effect on *SCN5A* activation. Interestingly, while *IRX5* and *SCN5A* display a comparable
489 gradient of expression through the ventricular wall, as well as a between atria and ventricles,
490 *GATA4* has a more uniform pattern of expression. We thus hypothesized that GATA4 and IRX5
491 could act cooperatively where GATA4 may be important for basal expression of *SCN5A* in
492 human cardiomyocytes while IRX5 creates its gradients of expression in the heart. Genetic
493 expression and/or function abnormalities of *SCN5A* together with conduction defects, have
494 been previously linked to other rare arrhythmic diseases, such as Brugada syndrome [33,34].
495 Thus, the current study elaborating the role of IRX5 in the control of ventricular conduction
496 through the regulation of *SCN5A* presents a framework for future studies on its potential
497 implication in other complex disease such as Brugada syndrome.

498 **4.4 Study limitations**

499 Arrhythmic diseases often present with a wide spectrum of phenotypes, even among patients
500 belonging to the same family. The individual genetic background is thought to play a major
501 role in this heterogeneity. In the context of hiPSC-based disease modeling, the use of isogenic
502 control, where the genetic variant has been corrected in the patient iPSC cell line, is increasingly

503 employed. The present study aimed at dissecting *IRX5* regulatory mechanisms of human
504 cardiac electrical function by modeling HMMS. Therefore, we chose to perform a comparative
505 analysis between control and two hiPSC lines obtained from two HMMS patients belonging to
506 different families and harboring different LOF mutations in *IRX5*. For all studied parameters,
507 similar results have been obtained for both types of mutated hiPS-CMs as compared to control
508 cells, strongly supporting a specific role for *IRX5* in the pathological phenotype and thereby
509 minimizing the relevance of using isogenic controls.

510 **5. Conclusion**

511 In conclusion, hiPS-CMs generated from patients with rare mutations in *IRX5* recapitulated
512 their clinical features of ventricular depolarization delay. Furthermore, a role for this
513 transcription factor in the orchestration of the gene expression program governing ventricular
514 electrical depolarization in human, was uncovered, bringing to light a new potential option for
515 therapeutic intervention.

516 **Acknowledgments:**

517 The authors would like to thank the Genomics and Bioinformatics Core Facility (GenoBiRD,
518 Biogenouest), the Cytometry facility (CytoCell), the iPS core facility, and the Cellular and
519 Tissular Imaging Core Facility (MicroPICell) of Nantes University, for their technical support.
520 The authors also would like to thank Dan Roden for the gift of SCN5A plasmids, and Sophie
521 Demolombe for helping with mouse studies.

522 **Sources of Funding:**

523 This work was funded by grants from The National Research Agency [HEART iPS ANR-15-
524 CE14-0019-01], and *La Fédération Française de Cardiologie*. Nathalie Gaborit was laureate
525 of fellowships from Fondation Lefoulon-Delalande and International Incoming Fellowship
526 FP7-PEOPLE-2012-IIF [PIIF-GA-2012-331436]. Zeina R. Al Sayed is supported by Eiffel
527 scholarship program of Excellence (Campus France), by Doctoral School of Science and
528 Technology-Lebanese University and The Fondation Genavie.

529 **Conflict of interest:** None declared.

530 **Authors contributions:**

531 Zeina R. Al-Sayed contributed to the acquisition, interpretation of data, and writing of the
532 report; Robin Canac contributed to data acquisition; Bastien Cimarosti contributed to data
533 acquisition; Carine Bonnard contributed to clinical data acquisition; Hanan Hamamy
534 contributed to clinical data acquisition; Hulya Kayserili contributed to clinical data acquisition;
535 Aurore Girardeau contributed to data acquisition; Mariam Jouni contributed to data acquisition
536 Nicolas Jacob contributed to data acquisition; Anne Gaignerie contributed to data acquisition
537 Caroline Chariou contributed to data acquisition; Laurent David contributed to data acquisition
538 Virginie Forest contributed to data acquisition; Céline Marionneau contributed to data
539 acquisition; Gildas Loussouarn contributed to data analysis, and writing of the report;
540 Guillaume Lamirault contributed to data analysis, and writing of the report; Bruno Reversade
541 contributed to clinical data acquisition; Kazem Zibara contributed to the writing of the report
542 Patricia Lemarchand contributed to the study design, interpretation of the data, and writing of
543 the report; Nathalie Gaborit contributed to the study design, interpretation of the data, and
544 writing of the report.

545 All authors discussed the results and contributed and approved the final manuscript.

546

547 **References**

- 548 1. Pazoki R, Wilde AAM, Bezzina CR. Genetic Basis of Ventricular Arrhythmias. *Curr*
549 *Cardiovasc Risk Rep.* 2010;4:454–60.
- 550 2. Gourraud J-B, Barc J, Thollet A, Le Scouarnec S, Le Marec H, Schott J-J, Redon R,
551 Probst V. The Brugada Syndrome: A Rare Arrhythmia Disorder with Complex
552 Inheritance. *Front Cardiovasc Med.* 2016;3:9.
- 553 3. Van Weerd JH, Christoffels VM. The formation and function of the cardiac conduction
554 system. *Development.* 2016;143:197–210.
- 555 4. Van Eif VWW, Devalla HD, Boink GJJ, Christoffels VM. Transcriptional regulation of
556 the cardiac conduction system. *Nat Rev Cardiol.* 2018.
- 557 5. Hu W, Xin Y, Zhang L, Hu J, Sun Y, Zhao Y. Iroquois Homeodomain transcription
558 factors in ventricular conduction system and arrhythmia. *Int J Med Sci.* 2018;15:808–15.
- 559 6. Hamamy HA, Teebi AS, Oudjhane K, Shegem N, Ajlouni K. Severe hypertelorism,
560 midface prominence, prominent/simple ears, severe myopia, borderline intelligence, and
561 bone fragility in two brothers: New syndrome? *Am J Med Genet A.* 2007;143A:229–34.
- 562 7. Bonnard C, Strobl AC, Shboul M, Lee H, Merriman B, Nelson SF, Ababneh OH, Uz E,
563 Güran T, Kayserili H, Hamamy H, Reversade B. Mutations in IRX5 impair craniofacial
564 development and germ cell migration via SDF1. *Nat Genet.* 2012;44:709–13.
- 565 8. Costantini DL, Arruda EP, Agarwal P, Kim K-H, Zhu Y, Zhu W, Lebel M, Cheng CW,
566 Park CY, Pierce SA, Guerchicoff A, Pollevick GD, Chan TY, Kabir MG, Cheng SH,
567 Husain M, Antzelevitch C, Srivastava D, Gross GJ, Hui C, Backx PH, Bruneau BG. The
568 Homeodomain Transcription Factor Irx5 Establishes the Mouse Cardiac Ventricular
569 Repolarization Gradient. *Cell.* 2005;123:347–58.
- 570 9. Zhang S-S, Kim K-H, Rosen A, Smyth JW, Sakuma R, Delgado-Olguín P, Davis M, Chi
571 NC, Puvindran V, Gaborit N, Sukonnik T, Wylie JN, Brand-Arzamendi K, Farman GP,
572 Kim J, Rose RA, Marsden PA, Zhu Y, Zhou Y-Q, Miquerol L, Henkelman RM, Stainier
573 DYR, Shaw RM, Hui C, Bruneau BG, Backx PH. Iroquois homeobox gene 3 establishes
574 fast conduction in the cardiac His–Purkinje network. *Proc Natl Acad Sci.*
575 2011;108:13576–81.
- 576 10. Kim K-H, Rosen A, Hussein SMI, Puvindran V, Korogyi AS, Chiarello C, Nagy A, Hui
577 C, Backx PH. Irx3 is required for postnatal maturation of the mouse ventricular
578 conduction system. *Sci Rep.* 2016;6:19197.
- 579 11. Marionneau C, Couette B, Liu J, Li H, Mangoni ME, Nargeot J, Lei M, Escande D,
580 Demolombe S. Specific pattern of ionic channel gene expression associated with
581 pacemaker activity in the mouse heart. *J Physiol.* 2005;562:223–34.
- 582 12. Jouni M, Si-Tayeb K, Es-Salah-Lamoureux Z, Latypova X, Champon B, Caillaud A,
583 Rungoat A, Charpentier F, Loussouarn G, Baró I, Zibara K, Lemarchand P, Gaborit N.
584 Toward Personalized Medicine: Using Cardiomyocytes Differentiated From Urine-
585 Derived Pluripotent Stem Cells to Recapitulate Electrophysiological Characteristics of
586 Type 2 Long QT Syndrome. *J Am Heart Assoc.* 2015;4:e002159.

- 587 13. Es-Salah-Lamoureux Z, Jouni M, Malak OA, Belbachir N, Sayed ZRA, Gandon-Renard
588 M, Lamirault G, Gauthier C, Baró I, Charpentier F, Zibara K, Lemarchand P, Beaumelle
589 B, Gaborit N, Loussouarn G. HIV-Tat induces a decrease in IKr and IKs via reduction in
590 phosphatidylinositol-(4,5)-bisphosphate availability. *J Mol Cell Cardiol.* 2016;99:1–13.
- 591 14. Wang W-X, Danaher RJ, Miller CS, Berger JR, Nubia VG, Wilfred BS, Neltner JH,
592 Norris CM, Nelson PT. Expression of miR-15/107 family microRNAs in human tissues
593 and cultured rat brain cells. *Genomics Proteomics Bioinformatics.* 2014;12:19–30.
- 594 15. Mestdagh P, Van Vlierberghe P, De Weer A, Muth D, Westermann F, Speleman F,
595 Vandesompele J. A novel and universal method for microRNA RT-qPCR data
596 normalization. *Genome Biol.* 2009;10:R64.
- 597 16. Bockmeyer CL, Säuberlich K, Wittig J, Eßer M, Roeder SS, Vester U, Hoyer PF,
598 Agustian PA, Zeuschner P, Amann K, Daniel C, Becker JU. Comparison of different
599 normalization strategies for the analysis of glomerular microRNAs in IgA nephropathy.
600 *Sci Rep.* 2016;6:31992.
- 601 17. Kilens S, Meistermann D, Moreno D, Chariou C, Gaignerie A, Reignier A, Lelièvre Y,
602 Casanova M, Vallot C, Nedellec S, Flippe L, Firmin J, Song J, Charpentier E, Lammers
603 J, Donnart A, Marec N, Deb W, Bihouée A, Caignec CL, Pecqueur C, Redon R, Barrière
604 P, Bourdon J, Pasque V, Soumillon M, Mikkelsen TS, Rougeulle C, Fréour T, David L.
605 Parallel derivation of isogenic human primed and naive induced pluripotent stem cells.
606 *Nat Commun.* 2018;9:360.
- 607 18. Croft D, Mundo AF, Haw R, Milacic M, Weiser J, Wu G, Caudy M, Garapati P,
608 Gillespie M, Kamdar MR, Jassal B, Jupe S, Matthews L, May B, Palatnik S, Rothfels K,
609 Shamovsky V, Song H, Williams M, Birney E, Hermjakob H, Stein L, D’Eustachio P.
610 The Reactome pathway knowledgebase. *Nucleic Acids Res.* 2014;42:D472–7.
- 611 19. Fabregat A, Korninger F, Viteri G, Sidiropoulos K, Marin-Garcia P, Ping P, Wu G, Stein
612 L, D’Eustachio P, Hermjakob H. Reactome graph database: Efficient access to complex
613 pathway data. *PLoS Comput Biol.* 2018;14:e1005968.
- 614 20. Medina PP, Nolde M, Slack FJ. OncomiR addiction in an in vivo model of microRNA-
615 21-induced pre-B-cell lymphoma. *Nature.* 2010;467:86–90.
- 616 21. Sartor MA, Leikauf GD, Medvedovic M. LRpath: a logistic regression approach for
617 identifying enriched biological groups in gene expression data. *Bioinforma Oxf Engl.*
618 2009;25(2):211–7.
- 619 22. Gaborit N, Varro A, Le Bouter S, Szuts V, Escande D, Nattel S, Demolombe S. Gender-
620 related differences in ion-channel and transporter subunit expression in non-diseased
621 human hearts. *J Mol Cell Cardiol.* 2010;49:639–46.
- 622 23. Biloni A, Craig G, Hill C, McNeill H. Iroquois transcription factors recognize a unique
623 motif to mediate transcriptional repression in vivo. *Proc Natl Acad Sci U S A.*
624 2005;102:14671–6.
- 625 24. Berger MF, Badis G, Gehrke AR, Talukder S, Philippakis AA, Peña-Castillo L, Alleyne
626 TM, Mnaimneh S, Botvinnik OB, Chan ET, Khalid F, Zhang W, Newburger D, Jaeger
627 SA, Morris QD, Bulyk ML, Hughes TR. Variation in Homeodomain DNA Binding

- 628 Revealed by High-Resolution Analysis of Sequence Preferences. *Cell*. 2008;133:1266–
629 76.
- 630 25. Noyes MB, Christensen RG, Wakabayashi A, Stormo GD, Brodsky MH, Wolfe SA.
631 Analysis of Homeodomain Specificities Allows the Family-wide Prediction of Preferred
632 Recognition Sites. *Cell*. 2008;133:1277–89.
- 633 26. Putten M van, E RM, Mengarelli I, Guan K, Zegers JG, Ginneken V, G AC, Verkerk
634 AO, Wilders R. Ion channelopathies in human induced pluripotent stem cell derived
635 cardiomyocytes: a dynamic clamp study with virtual IK1. *Front Physiol*. 2015;6:7.
- 636 27. Tarradas A, Pinsach-Abuin M, Mackintosh C, Llorà-Batlle O, Pérez-Serra A, Batlle M,
637 Pérez-Villa F, Zimmer T, Garcia-Bassets I, Brugada R, Beltran-Alvarez P, Pagans S.
638 Transcriptional regulation of the sodium channel gene (SCN5A) by GATA4 in human
639 heart. *J Mol Cell Cardiol*. 2017;102:74–82.
- 640 28. Giacomelli E, Mummery CL, Bellin M. Human heart disease: lessons from human
641 pluripotent stem cell-derived cardiomyocytes. *Cell Mol Life Sci CMLS*. 2017;74:3711–
642 39.
- 643 29. Ang Y-S, Rivas RN, Ribeiro AJS, Srivas R, Rivera J, Stone NR, Pratt K, Mohamed
644 TMA, Fu J-D, Spencer CI, Tippens ND, Li M, Narasimha A, Radzinsky E, Moon-Grady
645 AJ, Yu H, Pruitt BL, Snyder MP, Srivastava D. Disease Model of GATA4 Mutation
646 Reveals Transcription Factor Cooperativity in Human Cardiogenesis. *Cell*.
647 2016;167:1734-1749.e22.
- 648 30. Caballero R, Utrilla RG, Amorós I, Matamoros M, Pérez-Hernández M, Tinaquero D,
649 Alfayate S, Nieto-Marín P, Guerrero-Serna G, Liu Q-H, Ramos-Mondragón R, Ponce-
650 Balbuena D, Herron T, Campbell KF, Filgueiras-Rama D, Peinado R, López-Sendón JL,
651 Jalife J, Delpón E, Tamargo J. Tbx20 controls the expression of the KCNH2 gene and of
652 hERG channels. *Proc Natl Acad Sci*. 2017;114:E416–25.
- 653 31. Muszkiewicz A, Britton OJ, Gemmell P, Passini E, Sánchez C, Zhou X, Carusi A, Quinn
654 TA, Burrage K, Bueno-Orovio A, Rodriguez B. Variability in cardiac electrophysiology:
655 Using experimentally-calibrated populations of models to move beyond the single
656 virtual physiological human paradigm. *Prog Biophys Mol Biol*. 2016;120:115–27.
- 657 32. Gaborit N, Sakuma R, Wylie JN, Kim K-H, Zhang S-S, Hui C-C, Bruneau BG.
658 Cooperative and antagonistic roles for Irx3 and Irx5 in cardiac morphogenesis and
659 postnatal physiology. *Dev Camb Engl*. 2012;139:4007–19.
- 660 33. Gaborit N, Wichter T, Varro A, Szuts V, Lamirault G, Eckardt L, Paul M, Breithardt G,
661 Schulze-Bahr E, Escande D, Nattel S, Demolombe S. Transcriptional profiling of ion
662 channel genes in Brugada syndrome and other right ventricular arrhythmogenic diseases.
663 *Eur Heart J*. 2009;30:487–96.
- 664 34. Juang J-MJ, Tsai C-T, Lin L-Y, Liu Y-B, Yu C-C, Hwang J-J, Chen J-J, Chiu F-C, Chen
665 W-J, Tseng C-D, Chiang F-T, Yeh H-M, Sherri Yeh S-F, Lai L-P, Lin J-L. Unique
666 clinical characteristics and SCN5A mutations in patients with Brugada syndrome in
667 Taiwan. *J Formos Med Assoc*. 2015;114:620–6.

668

669

670 **Figure legends :**

671 **Figure 1: IRX5 TF and conduction genes expression in human cardiac tissues.**

- 672 A. Heatmap displaying expression level of 212 cardiac genes (ion channels and TFs) in murine
673 atrial and ventricular tissues measured by TLDA ($-\Delta\text{Ct}$), and in human atrial and left
674 ventricular samples (GTEX). Murine genes were clustered using hierarchical ascending
675 method with an uncentered correlation metric and average linkage. Heatmap of the same
676 genes was obtained in human tissues based on the murine cluster, in a supervised hierarchical
677 manner. Yellow and blue indicate high and low expression levels respectively.
678 Representative genes of the ventricular-specific gene cluster are listed in the yellow box.
- 679 B. Expression level of genes encoding sodium channels and gap junction proteins in left
680 ventricular tissues. Samples were ordered according to their IRX5 expression levels (purple
681 gradient). Pearson correlation between each sodium channel or gap junction gene and IRX5
682 expression profiles are shown using pink gradients.
- 683 C. Representative immunoblots of IRX5, $\text{Na}_v1.5$ and Cx40 levels in human protein lysates of
684 ventricular sub-endocardial (Endo) and sub-epicardial (Epi) samples obtained from three
685 human left (LV) and right ventricles (RV). Corresponding averaged IRX5, $\text{Na}_v1.5$ and Cx40
686 protein expression levels obtained from tissue samples of three individuals, normalized to
687 Stain free.

688 **Figure 2: Characterization of IRX5-mutated hiPS-cardiomyocytes**

- 689 A. Principal Component Analysis (PCA) of 21 hiPSC samples (in pink) and 19 hiPS-CM
690 samples (in blue) based on their expression pattern of 27106 analyzed transcripts (3'SRP
691 data).
- 692 B. Correlation matrix of hiPSCs and hiPS-CMs expression profiles (same samples as in A).
693 Samples were clustered using an ascending hierarchical method with Pearson as metric and
694 ward.D2 linkage. Yellow and orange indicate high and low correlation, respectively.
- 695 C. Heatmap showing expression levels for 9661 differentially expressed genes between hiPSCs
696 and hiPS-CMs (same samples as in A). Genes were clustered using a hierarchical ascending
697 method with an uncentered correlation metric and average linkage. Yellow and blue indicate
698 high and low levels respectively.
- 699 D. Illustrative immunostainings of IRX5 (red) and Troponin I (green) in hiPS-CMs, merged
700 with a nuclear staining using DAPI (blue). To confirm nuclear localization of IRX5, XZ
701 orthogonal planes are illustrated next to each picture.

- 702 E. Representative traces and distribution (as percentage) of nodal-like, atrial-like and
703 ventricular-like cells, based on the analysis of AP parameters in spontaneously beating hiPS-
704 CMs.
- 705 F. *IRX5* mRNA expression level in control and mutated hiPS-CMs at day 28 of cardiac
706 differentiation using TaqMan® technique (Ctrl: n=22; A150P: n=8; N166K: n=14).
- 707 G. Nuclear expression level of *IRX5* protein in control and mutated hiPS-CMs, normalized to
708 Stain free. Representative immunoblot showing *IRX5* expression in the nuclear protein
709 fraction (Ctrl: n=11; A150P: n=10; N166K: n=11).

710 **Figure 3: Transcriptomic aberrations in *IRX5*-mutated cardiomyocytes.**

- 711 A. Heatmap showing hierarchical clustering of expression profiles of the 745 differentially
712 expressed genes obtained by 3'SRP in control (Ctrl) and *IRX5*-mutated hiPS-CMs at day 28
713 of differentiation. 41% and 59% genes were upregulated and downregulated in *IRX5*-
714 mutated hiPS-CMs, respectively. Yellow and blue represent high and low expression levels
715 respectively. Relevant genes implicated in the function or regulation of cardiac electrical
716 conduction are highlighted on the right.
- 717 B. Histograms showing expression levels of differentially expressed genes in *IRX5*-mutated
718 hiPS-CMs (n=9) identified using TLDA, as compared to control hiPS-CMs (n=12). * and
719 **: p<0.05 and p<0.01 vs. control, respectively (*t* test).
- 720 C. Top panel: Functional annotation of differentially expressed genes at day 28 of
721 differentiation, obtained by 3'SRP and TaqMan. Histograms showing over-represented
722 Reactome pathways. Only pathways with Enrichment Score>2 and p<0.05 are shown.
723 Bottom panel: Detailed muscle contraction pathway is represented.

724 **Figure 4: Impaired expression of *GJA5* and *SCN5A* in *IRX5*-mutated hiPS-CMs.**

- 725 A. TaqMan® analysis showing mRNA expression of *SCN5A* and *GJA5* in control (n=21),
726 A150P (n=8) and N166K (n=12) *IRX5*-mutated hiPS-CMs. Cts were normalized to *ACTB*
727 and $2^{-\Delta\Delta C_t}$ was calculated. * and **: p<0.05 and p<0.01 vs. control, respectively (*t* test).
- 728 B. Representative immunoblots for $Na_v1.5$ and Cx40 and ratios of $Na_v1.5$ and Cx40 expression
729 levels normalized to Transferrin receptor (TFRC). Blots were quantified using Image Lab
730 software. ** and ***: p<0.01 and p<0.001 vs. control, respectively (*t* test). Ctrl: n=38;
731 A150P: n=22; N166K: n=22.

732 C. Representative confocal images for immunostainings of Na_v1.5 and Cx40 (green) in
733 Troponin I positive (red) control and *IRX5*-mutated hiPS-CMs. Nuclei are stained in blue
734 using DAPI.

735 **Figure 5: *IRX5* loss-of-function leads to a slower upstroke velocity via reduction of I_{Na}**

736 A. Top panel: representative traces of ventricular APs measured in *IRX5*-A150P and -N166K
737 mutated and control hiPS-CMs paced at 700ms cycle length with their corresponding first
738 derivatives of AP upstroke velocity (arrows). Bottom panel: Box whisker plots of maximum
739 upstroke velocities of ventricular APs when pacing at 700ms cycle length without *in-silico*
740 I_{K1} injection.

741 B. Resting membrane potentials (RMPs) measured from ventricular APs paced at 700ms cycle
742 length with or without *in-silico* I_{K1} injection. Mean and SEM are indicated; n: same as in A
743 and C.

744 C. Top panel: representative traces of ventricular APs measured in A150P and N166K *IRX5*-
745 mutated and control hiPS-CMs paced at 700ms cycle length with their corresponding first
746 derivatives of AP upstroke velocities (arrows). Bottom panel: Box whisker plots of
747 maximum upstroke velocities of ventricular APs when pacing at 700ms cycle length and
748 under dynamic clamp with *in-silico* I_{K1} injection. * and **: p<0.05 and p<0.01 vs. control,
749 respectively (*t* test).

750 D. Representative traces of I_{Na}-TTX-sensitive and I_{Ca,L}-Nifedipine-sensitive in control hiPS-
751 CMs, obtained by subtraction of the current recorded before and after application of the
752 inhibitors, when applying typical ventricular-like AP voltages, depicted on top.

753 E. Superimposed representative traces of I_{Na} recorded when applying the depicted voltage-
754 clamp protocol, and mean current densities (pA/pF) vs. membrane potential (EM) recorded
755 in hiPS-CMs. *** and #### p<0.001 vs. control for respectively *IRX5*-A150P and -N166K
756 hiPS-CMs (Two-way Anova with Bonferroni post hoc test).

757 F. Superimposed representative traces of I_{Ca,L} recorded when applying the depicted voltage-
758 clamp protocol, and mean current densities (pA/pF) vs. membrane potential (EM) obtained
759 in hiPS-CMs.

760 **Figure 6: *IRX5* interacts with *SCN5A*, *GJA5* and *GJA1* promoters.**

761 A. Schematic representation of potential binding sites for *IRX5* (BS, in green; numbers indicate
762 position referring to TSS) on *SCN5A* promoter identified *in-silico*, and PCR amplification
763 using primers specific for each BS after hiPS-CMs chromatin immunoprecipitation (ChIP)
764 with an antibody against *IRX5*. Results are shown as ratio of the immunoprecipitated (IPed)

765 DNA relative to intergenic region (IR). TSS: transcription starting site; CP: core promoter.
766 #: $p < 0.05$ vs. IR in control samples (n=8); ***: $p < 0.001$ vs. control in IRX5-mutated
767 samples; A150P n=5 and N166K: n=7 (*t* test).

768 B and C. IRX5 interaction with *GJA5* and *GJA1* promoters, respectively, obtained as in A Ctrl:
769 n=6; A150P: n=5; N166K: n=7..

770 D. Dissociation constant (Kd) between IRX5 protein and *SCN5A* promoter obtained after
771 microscale thermophoresis (MST) test using constant concentration of IRX5 protein and
772 decreasing concentration of *SCN5A* promoter plasmids (from 650nM to 0.0099nM). Two
773 different plasmids containing parts of *SCN5A* promoter were used: BS2- Plasmid, from -261
774 to +613bp, that did not contain *IRX5 BS2*, and BS2+ Plasmid, from -261 to +1072bp, which
775 contained *IRX5 BS2*. Left panel, fitted curves issued using law of mass action. Right panel,
776 histograms showing mean and SEM Kd (n=3 per group).

777 E. Luciferase experiments in HEK293 cells cotransfected with BS2+ Plasmid, containing
778 *luciferase* cDNA under the control of *SCN5A* promoter region (from -261bp to +1072bp),
779 and with expressing vectors encoding wild-type (WT), A150P or N166K-mutated *IRX5*
780 cDNA. Firefly luciferase activity was normalized to Renilla activity (mean \pm SEM, n=3 per
781 group) and is shown as ratio vs. condition without IRX5 plasmid.

782 **Figure 7: IRX5 and GATA4 cooperate to regulate *SCN5A* expression.**

783 A. *GATA* transcripts expression ratios vs. *GATA5* (*GATA* TF with the lowest expression).
784 Transcript expression ratios were calculated using GTEx data for human ventricular tissues
785 and using TLDA analysis for control hiPS-CMs. Data are expressed as mean \pm SEM.

786 B. Representative western blots of IRX5 and GATA4 in control and IRX5-A150P mutated
787 hiPS-CM lysates immunoprecipitated with anti-IRX5 antibody. Quantification of the
788 amount of GATA4 co-immunoprecipitated with IRX5, in control and, IRX5-A150P and -
789 N166K mutated hiPS-CMs. Results are shown as ratios of the co-immunoprecipitated (IPed)
790 GATA4 normalized to the IPed IRX5 amounts (Ctrl: n=20; A150P: n=11; N166K: n=8).

791 C. Schematic representation of *IRX5* binding site (BS; green) and *GATA4* BS (pink) on *SCN5A*
792 promoter (numbers indicate position referring to TSS), and PCR amplification using primers
793 specific for each BS after hiPS-CMs CHIP with an antibody against IRX5. Results are shown
794 as ratio of the IPed DNA relative to intergenic region (IR). TSS: transcription starting site.
795 #: $p < 0.05$ vs. intergenic region (*t* test). Ctrl: n=7; A150P n=4 and N166K: n=6.

796 D. Luciferase experiments in HEK293 cells cotransfected with BS2- plasmid, containing
797 *luciferase* cDNA under the control of *SCN5A* promoter region (-261bp to +613bp) with

798 *GATA4 BSb* but not *IRX5 BS2* (white bars), or *BS2+* plasmid, containing *luciferase* cDNA
799 under the control of *SCN5A* promoter region (-261bp to +1072bp) with *GATA4 BSb* and
800 *IRX5 BS2* (green bars), and with the indicated *GATA4* or/and *IRX5* expressing plasmids.
801 Firefly luciferase activity was normalized to Renilla and is shown as ratio to its activity when
802 transfected with *SCN5A* plasmids only. *****: $p < 0.0001$ vs. condition with no *IRX5/GATA4*
803 plasmid; ### and #####: $p < 0.001$ and $p < 0.0001$ vs. condition with *GATA4* plasmid only;
804 \$\$\$: $p < 0.001$ vs. condition with *GATA4* + WT-*IRX5* plasmids (*t* test).

Figure 1

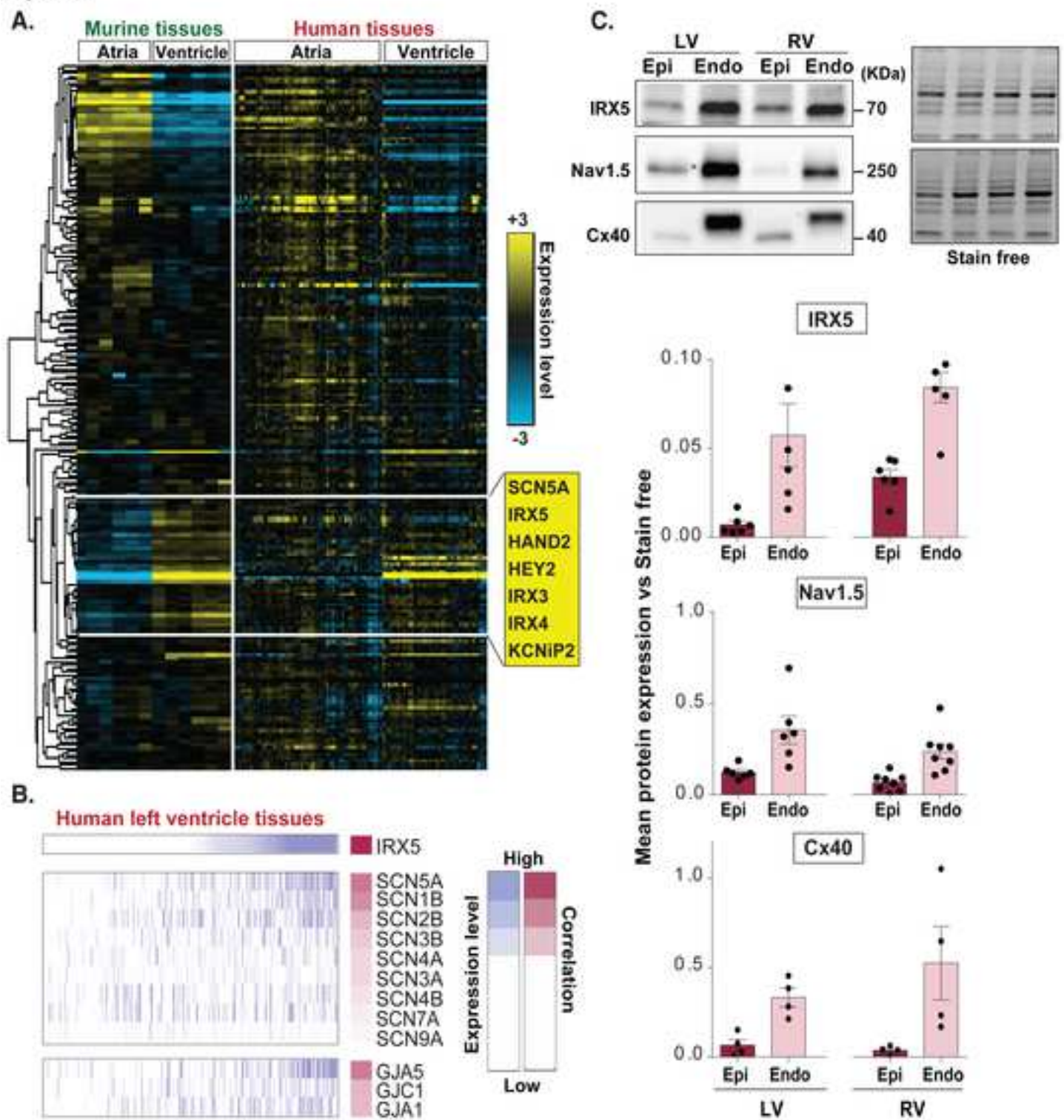


Figure 2

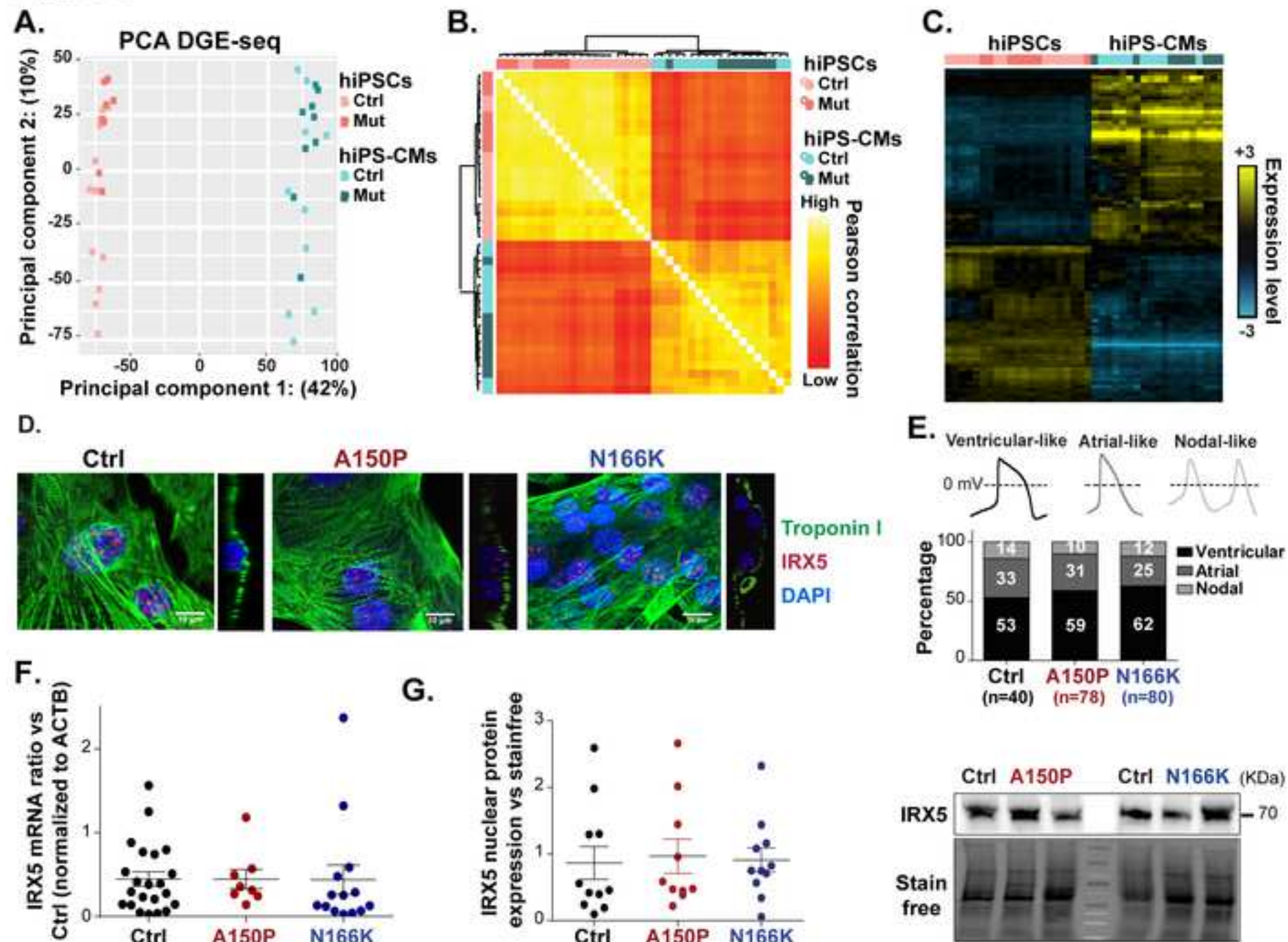


Figure 3

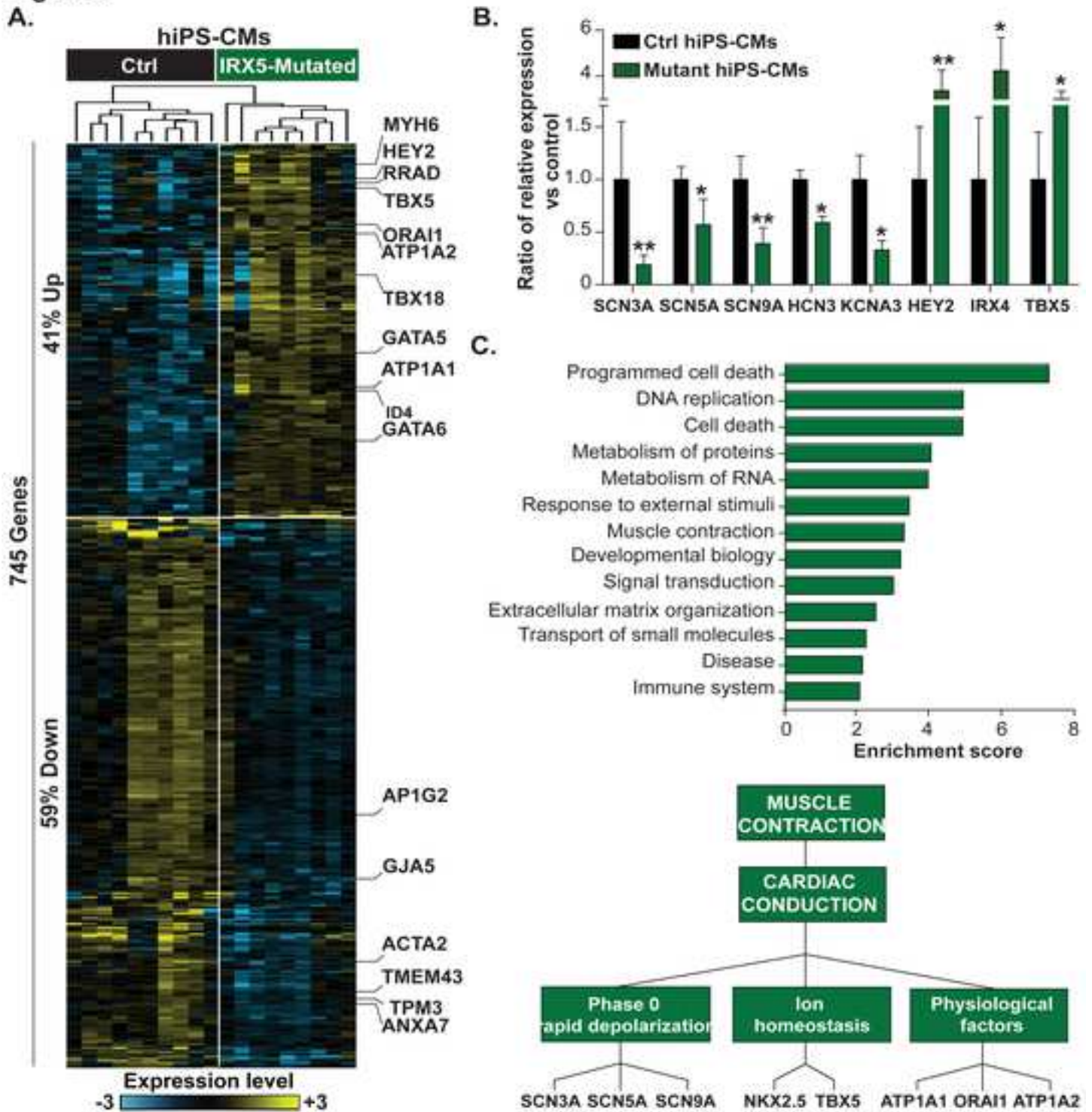


Figure 4

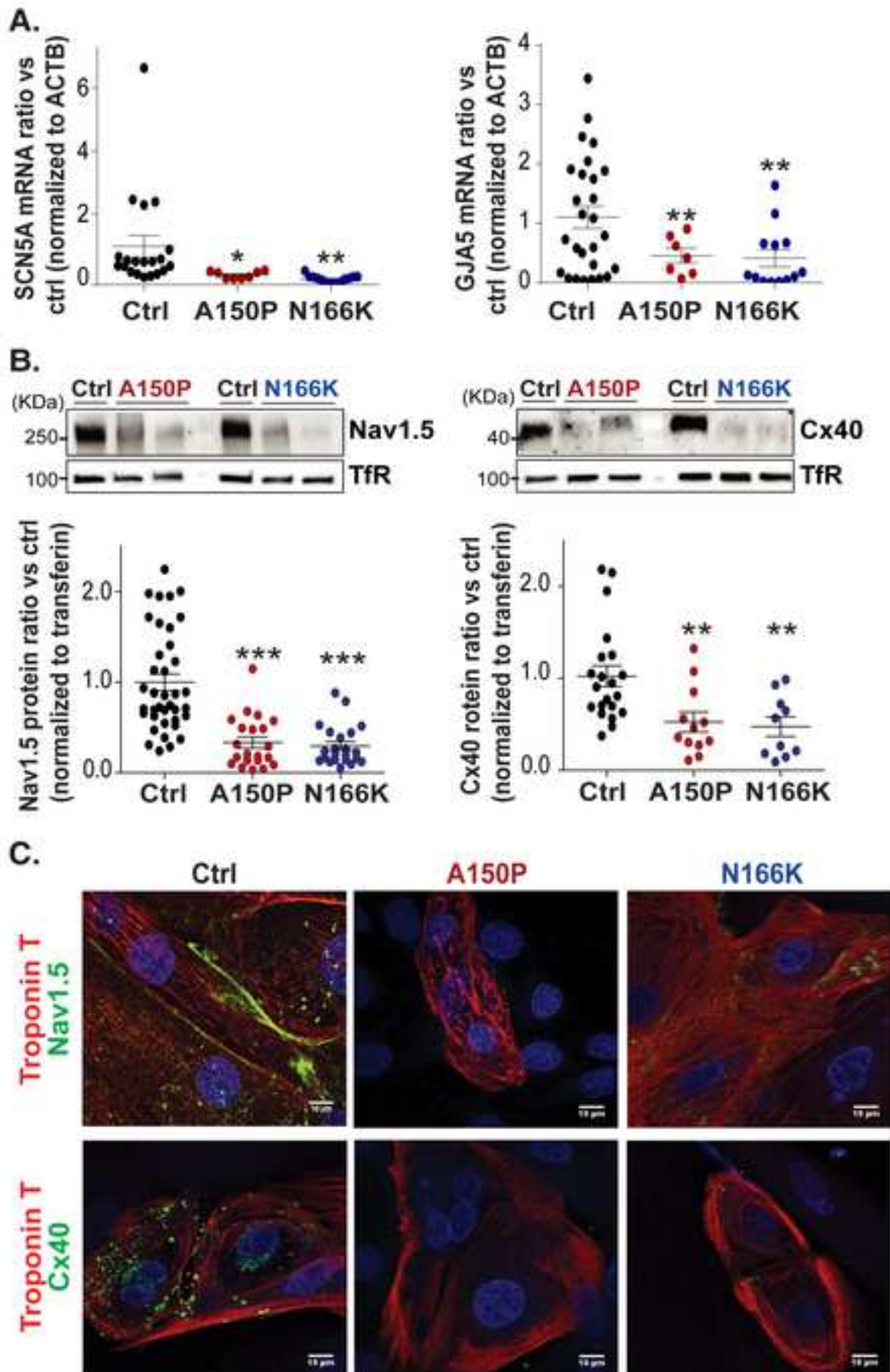


Figure 5

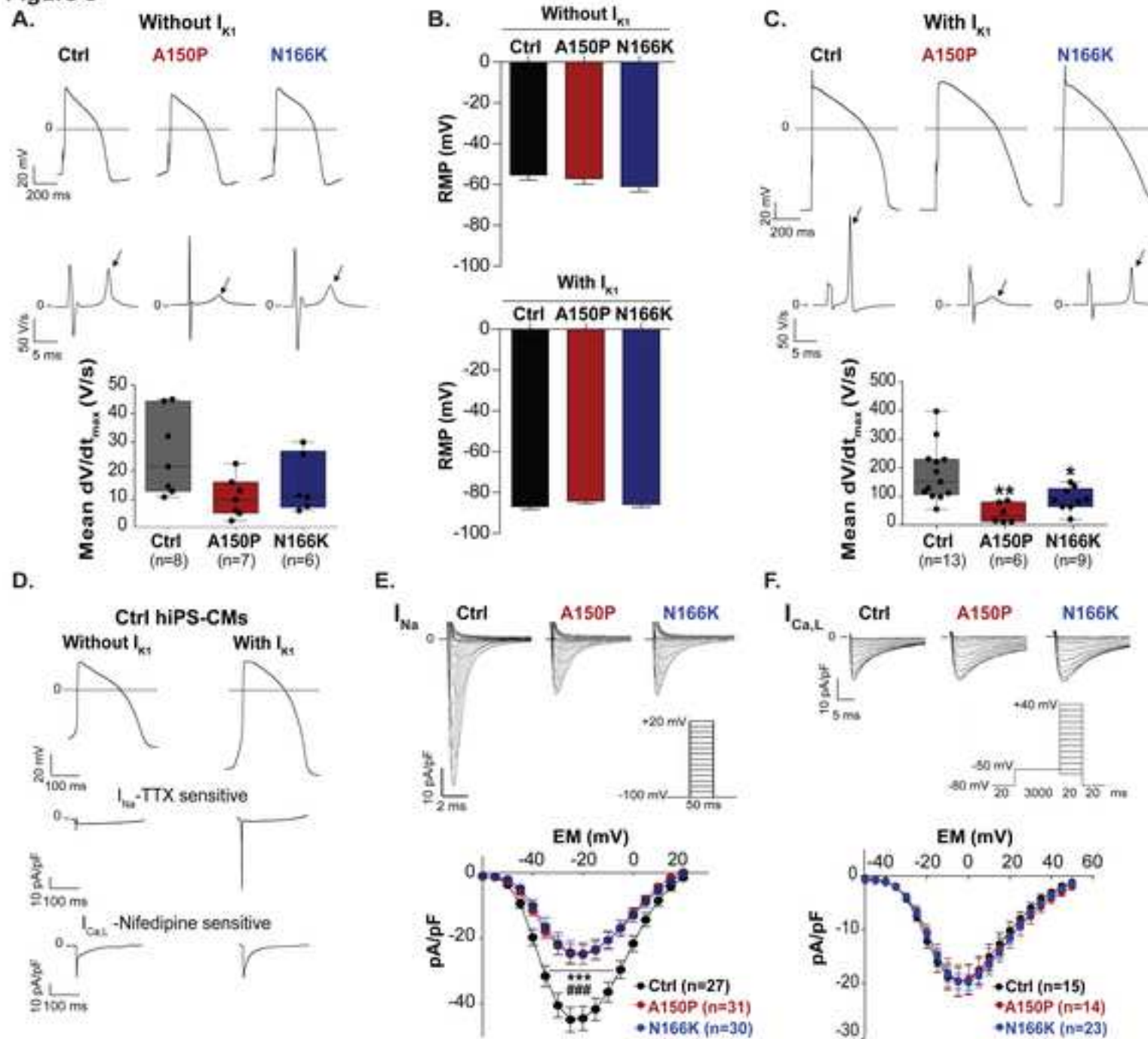


Figure 6

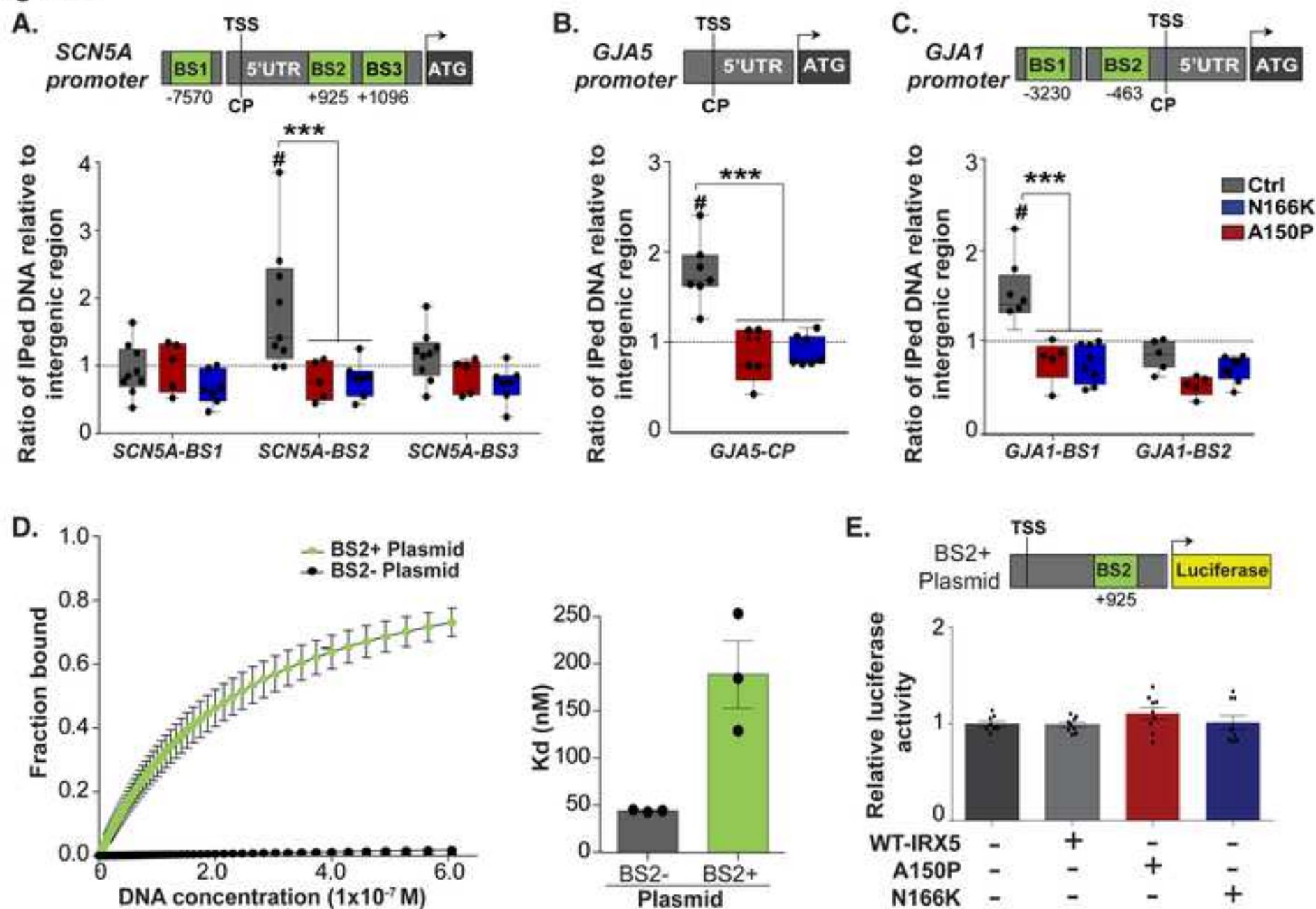
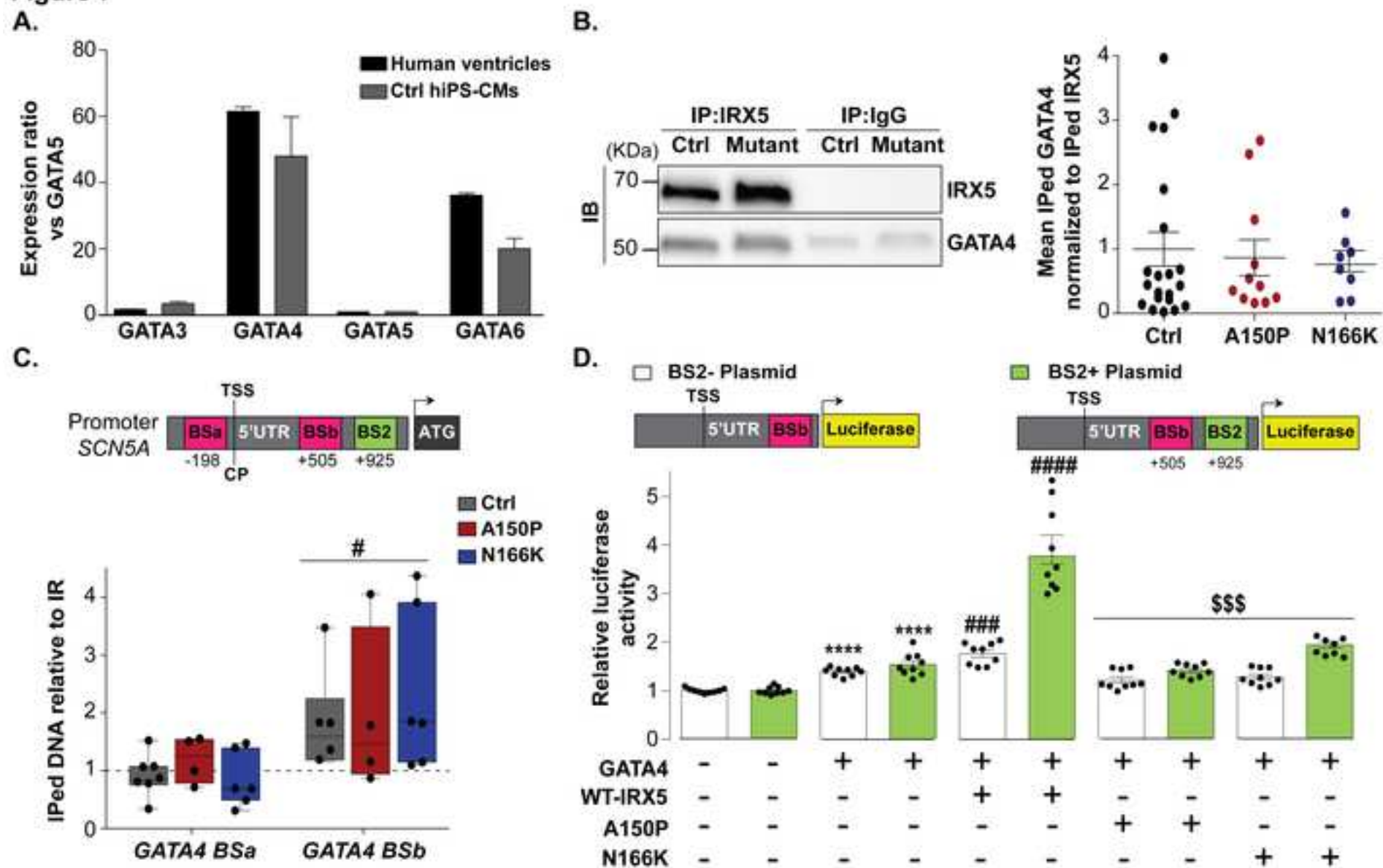


Figure 7



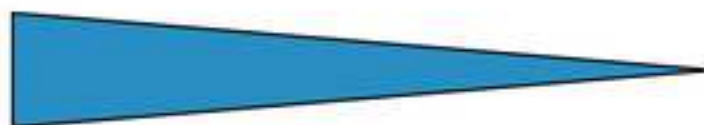


Ventricular wall

Endo

Epi

IRX5



GATA4



SCN5A



Conduction:

Faster

Slower

Human disease model of *IRX5* mutations reveals key role for this transcription factor in cardiac conduction

Zeina R Al Sayed et al.

SUPPLEMENTAL MATERIAL

Quantitative RT-PCR

Reverse transcription of 1 µg total RNA into cDNA was achieved using the high-capacity cDNA reverse transcription Kit (Thermo Fisher Scientific). Quantitative Polymerase Chain Reactions (qPCR) were executed in duplicates using TaqMan® PCR Universal Master Mix (Thermo Fisher Scientific). TaqMan probes targeting *IRX5* (Hs04334749_m1), *SCN5A* (Hs00165693_m1), *GJA5* (Hs00270952_s1), *GJA1* (Hs00748445_s1) and *MYH7* (Hs01110632_m1) were used. Threshold cycles (Cts) were normalized to *ACTB* (Hs99999903_m1).

Immunoblotting: 2 µl NuPAGE Sample Reducing Agent and 5 µl NuPAGE LDS Sample Buffer were added to 40 µg proteins. The protein running was performed in 4-15% precast polyacrylamide gels (Bio-Rad) and proteins were then transferred onto Trans-Blot® Turbo™ Nitrocellulose Transfer Packs (Bio-Rad). Membranes were blocked using 5% non-fat milk. Expression of Cx40, Cx43, GATA4, IRX5, and Nav1.5 was revealed using respectively anti-Cx40 (Santa Cruz), anti-Cx43 (Sigma-Aldrich), anti-GATA4 (Santa Cruz), anti-Irx5 (Sigma-Aldrich) and anti-Nav1.5 (Cell signaling), and adequate secondary antibodies (Santa Cruz). Blots were revealed using chemiluminescence camera (Bio-Rad). Proteins were quantified using Image Lab software and normalized using Stain free technology or using endogenous transferrin expression.

Chromatin immunoprecipitation (ChIP): At day 28 of differentiation, beating cardiomyocyte clusters were isolated and crosslinked using 11% formaldehyde during 10 min at RT. Fixation was then stopped using 2.5M glycine for 3 min on ice. After 3 washes with PBS, cell lysis was performed using lysis buffer (10% glycerol, 140 mM NaCl, 0.5% NP40, 0.25% Triton X-100, and 1 mM EDTA) at 4°C for 10 min on a rotating platform. The cell pellets were washed with a solution containing: 200 mM NaCl, 10 mM Tris Base HCl, 0.5 mM EGTA and 1 mM EDTA. Then, the pellets were resuspended in a low salt buffer (1% Triton X-100, 140 mM NaCl, 0.1% Na deoxycholate, 0.1% SDS and 1 mM EDTA) supplemented with protease inhibitors (Sigma-Aldrich). Chromatin was sonicated with Misonix S-4000

(Qsonica). After 10 min centrifugation at 14000 rpm, supernatants were collected and incubated overnight at 4°C with 4 µg of anti-IRX5 antibody. Protein G-coated dynabeads, pre-blocked with BSA, were then added and allowed to couple with antibody-protein-DNA complexes overnight at 4°C. The dynabeads were collected, washed and then resuspended in an elution buffer (1% SDS, 50 mM Tris HCl and 10 mM EDTA). The chromatin was eluted at 65°C and then reverse-crosslinked at 65°C overnight. The DNA was treated with RNase A (Thermo Fisher) and proteinase K, purified using phenol-chloroform-isoamyl alcohol (25:24:1) and precipitated with 100% ethanol, 5 M NaCl, and 0.15 µg/µl Glycogen. SYBER green qRT-PCR method was finally performed using the designed primers (Online Table 3) to test for enrichment of the targeted sequences. Results are shown as percentage of input.

Plasmid constructs

SCN5A promoter-luciferase construct, covering the region from -261 to +613 bp of the TSS (BS2- Plasmid), contains *GATA4 BSb* and is a kind gift from Dr. Dan Roden (Vanderbilt University, Nashville, TN, USA). A total of 459 bp were added to this construct to cover +1072 bp from TSS (BS2+ Plasmid) using the NEBuilder HiFi DNA assembly cloning kit (New England Biolabs) and following manufacturer's instructions. pCMV6-GATA4 Myc-tagged (RC210945; OriGene) and pCMV6-IRX5 GFP-tagged (RG234228; OriGene) vectors encode human GATA4 and IRX5, respectively. The A150P and N166K mutations were added to the IRX5 expressing vector using the Q5® Site-Directed Mutagenesis kit (New England Biolabs). The A150P was produced by G/C transversion at +448 using the following primers: Fw: GATCATGCTcCCATCATCACCAAGATG and Rv: TTCTCGCCCTTGGTG GGG. The N166K mutation was produced by C/A transversion at +498 using the following primers: Fw GGTTCGCCAAaGCGCGCCGGC and Rv: AGGTGGACACCTGGGTGAGGG.

Supplemental Figures:

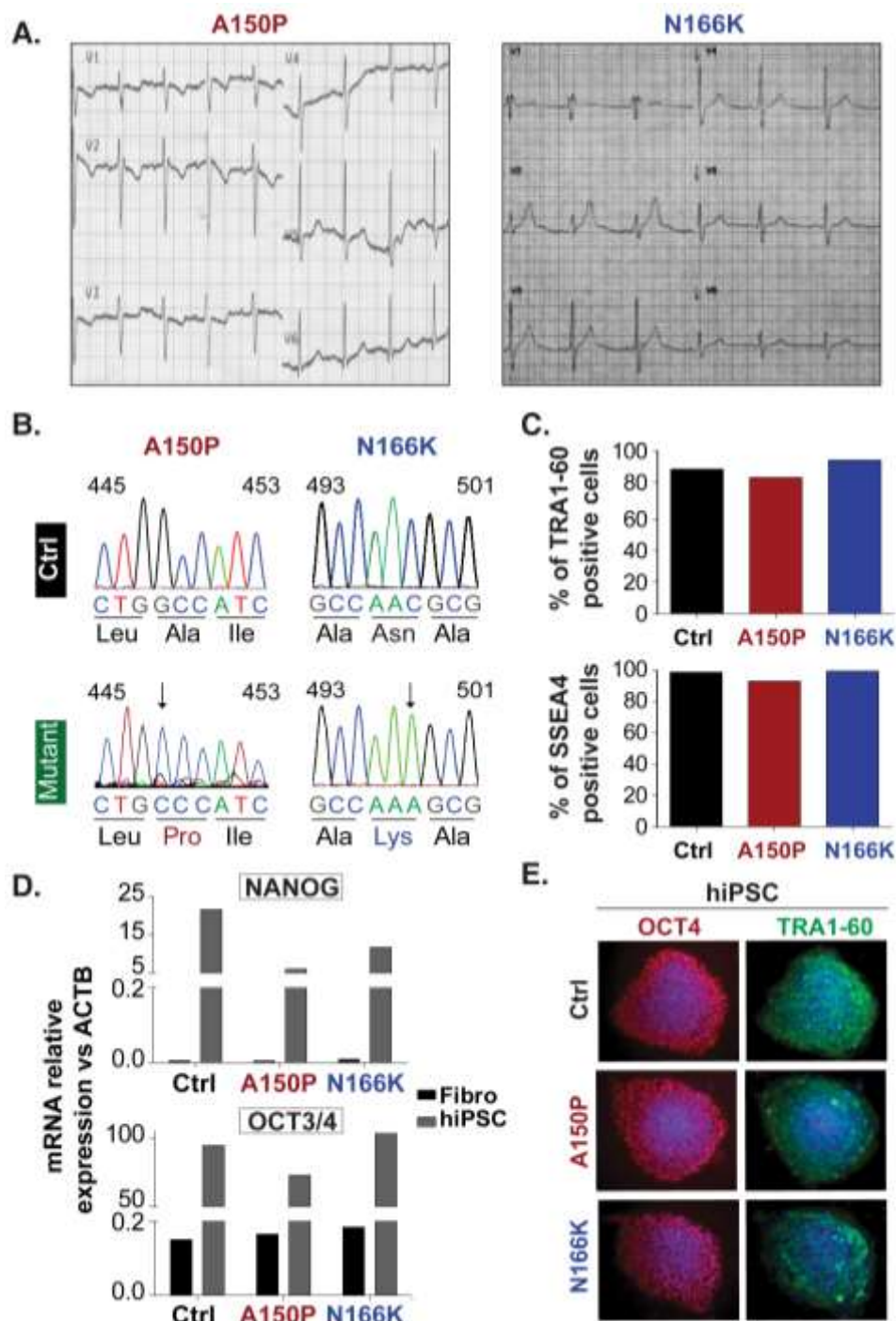


Figure S1: Validation of hiPSCs derived from Hamamy syndrome-affected patients.

- A. Leads V1 to V6 from electrocardiogram (ECG) of patients carrying A150P- and N166K-*IRX5* mutations. Conduction defect presented by Right Bundle Branch Block at the V1 lead and QRS prolongation is visible in both patient ECG.
- B. Genomic sequence chromatograms validate the presence of c.448G>C and c.498C>A *IRX5* mutations in mutant hiPSCs but not in control hiPSCs.

- C. Flow cytometry quantification of pluripotent stem cell markers TRA1-60 and SSEA4 in control and *IRX5*-mutated hiPSCs.
- D. mRNA expression levels of endogenous pluripotent stem cell markers, NANOG and OCT3/4, in control and *IRX5*-mutated hiPSCs as compared to their corresponding skin fibroblasts (Fibro) using TaqMan® technique.
- E. Representative immunostainings of endogenous OCT4 nuclear pluripotency marker and TRA1-60 pluripotency marker expressed at the membrane. Nuclei are stained in blue by DAPI.

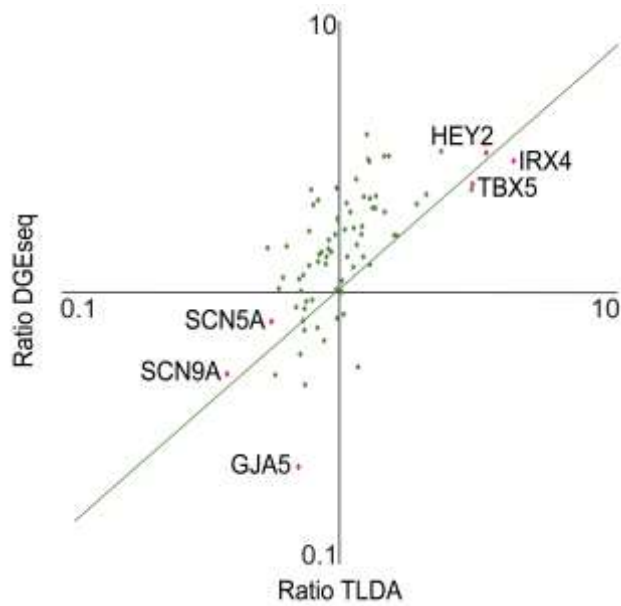


Figure S2: TLDA and 3'SRP data are correlated.

Ratios of mRNA expression in *IRX5*-mutated over control hiPS-CMs for 93 genes selected for TLDA analysis. For each gene, ratio obtained by TLDA was plotted in X coordinate and ratio obtained by 3'SRP was plotted in Y coordinate. Green Line represents identity line. Examples of genes relevant to cardiac conduction are shown in pink. For instance, *IRX4* increased according to both 3'SRP and TLDA (3X vs 4.2X, respectively) whereas *SCN5A*, *SCN9A* and *GJA5* decreased according to both 3'SRP and TLDA (1.3X vs 1.8X; 2X vs 2.5X and 4.3X vs 1.4X, respectively).

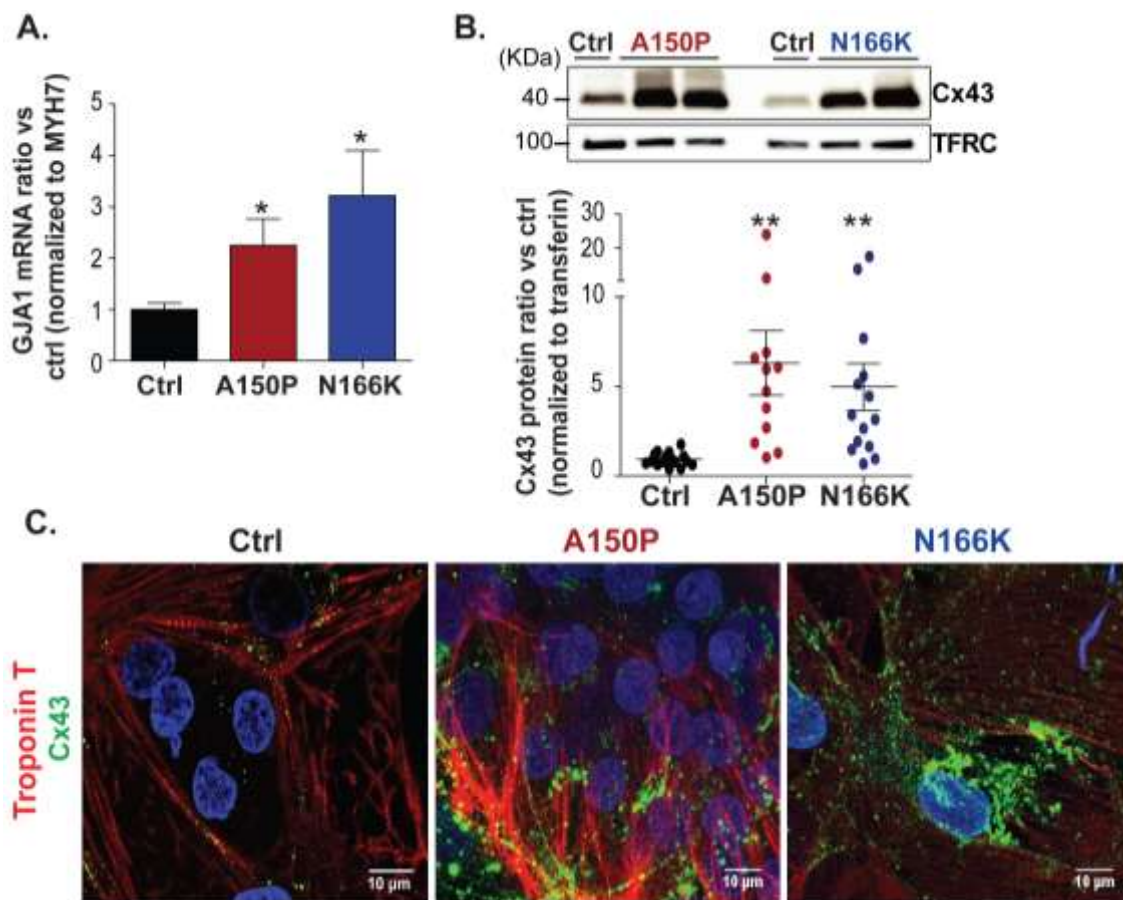


Figure S3: Cx43 ectopic expression in both A150P- and N166K-hiPS-CMs.

- A. TaqMan quantification of GJA1 transcript expression. Cts were normalized to MYH7, a myosin specific to ventricular cardiomyocytes. Ctrl n=19; A150P n=8; N166K n=8. * p<0.05 vs. control (*t* test).
- B. Representative immunoblot showing Cx43 protein expression with corresponding transferrin (transf) expression in A150P and N166K *IRX5*-mutated and control hiPS-CMs. Ratio of Cx43 expression level (normalized to transferrin expression level) in A150P (n=12) and N166K (n=14) *IRX5*-mutated hiPS-CMs vs. control hiPS-CMs (n=16). ** p<0.01 vs. control (*t* test).
- C. Immunostainings illustrating Cx43 expression and localization (green) in Troponin T (red) positive hiPS-CMs, merged with a nuclear staining using DAPI (blue)

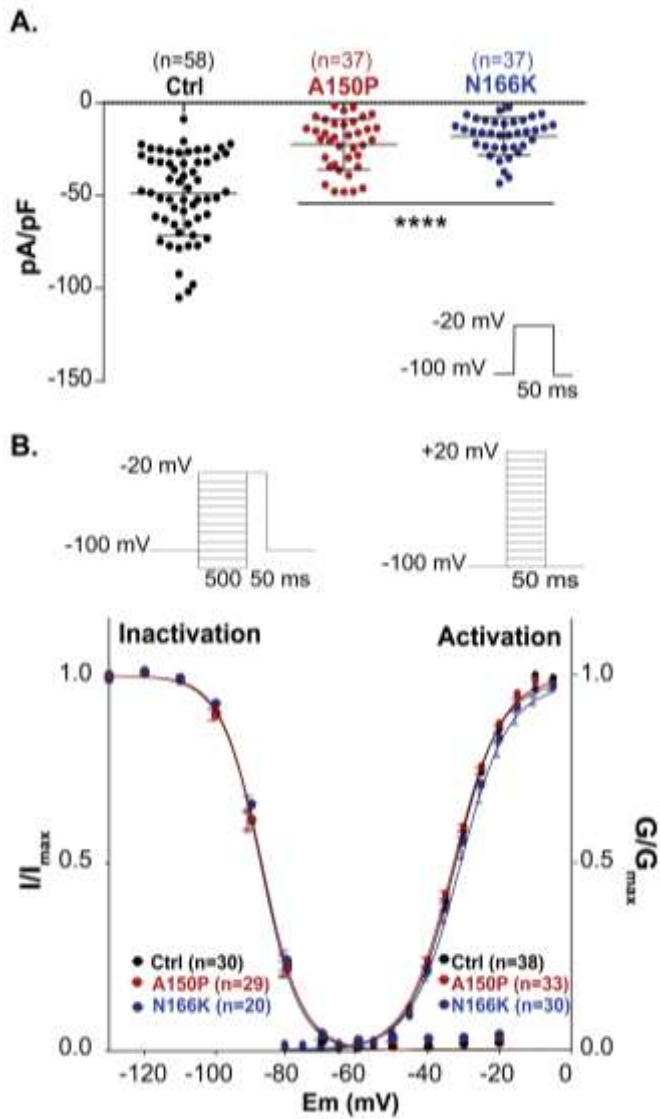


Figure S4: I_{Na} density was reduced in *IRX5*-mutated hiPS-CMs with no change in activation and inactivation parameters.

A. Current densities measured in control and *IRX5*-mutated hiPS-CMs, determined at -20 mV.

**** $p < 0.0001$ vs. control (t test).

B. I_{Na} voltage dependence of activation and steady-state inactivation (respective protocols depicted in insets).

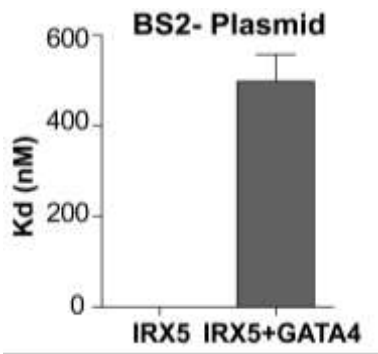


Figure S5: In contrast with IRX5 alone, the complex GATA4-IRX5 was able to bind to *SCN5A* plasmid lacking BS2

MST analysis of dissociation constant for interaction between *SCN5A* promoter (BS2- Plasmid) and IRX5 alone or IRX5 + GATA4. Protein lysates were prepared from HEK293T transfected with either IRX5-GFP only or both IRX5-GFP and GATA4 expressing vectors. Binding was tested with different concentrations of BS2- Plasmid containing *GATA4 BSb* but not *IRX5 BS2* (n=2 per group).

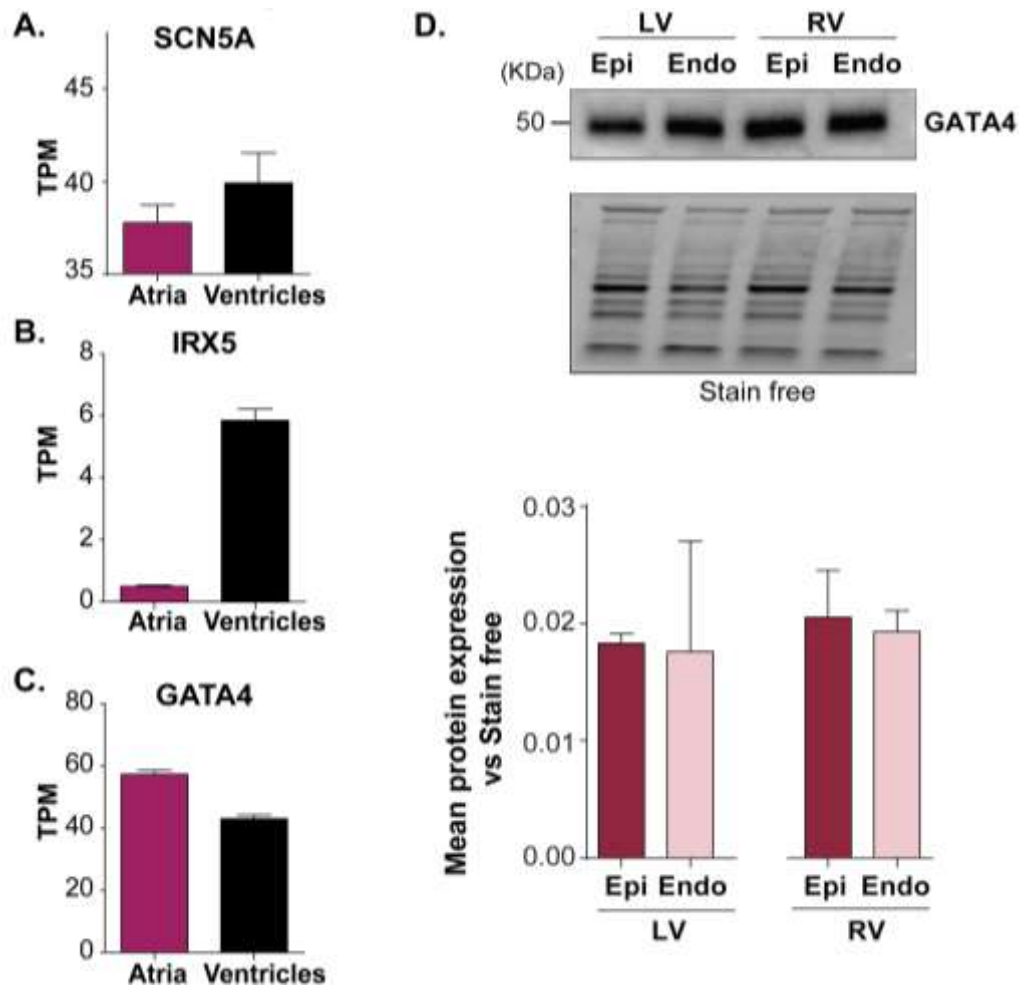


Figure S6: IRX5 but not GATA4 has a comparable expression profile to SCN5A.

A, B and C represents respectively transcriptomic profiles of SCN5A, IRX5 and GATA4 in atrial and ventricular human tissues, respectively. TPMs were obtained from GTEx database (n=297 and 303 for atrial and ventricular tissues, respectively).

D. Top: Representative immunoblot of GATA4 expression levels in protein lysates of ventricular sub-endocardial (Endo) and sub-epicardial (Epi) samples obtained from three human left (LV) and right ventricles (RV). Bottom: GATA4 protein expression level quantifications (n=3 per group), normalized to Stain free.

Supplemental Tables

Supplemental Table 1. Primer sequences used to validate mutations in mutant hiPSCs.

	Sequence
IRX5A150P-F	ccctgggatcgtacccttac
IRX5A150P-R	ggcgtccacgtcattttatt
IRX5N166K-F	aacgagcaccgcaagaac
IRX5N166K-R	gtcctcgtcgttcttctcca

Supplemental Table 1. A. Murine tissue TLDA probe references and corresponding genes. B. Human iPSCs TLDA probe references and corresponding genes.

A		B	
Transcription factors		Ion channels	
18S	Mm03928990_g1	18S	Mm03928990_g1
Arnt	Mm00507836_m1	Abcc9	Mm00441638_m1
Arntl	Mm00500226_m1	Actc1	Mm00477277_g1
Atf1	Mm00464368_m1	Ank2	Mm00618325_m1
Atf1	Mm00657594_m1	Atp1a1	Mm00523255_m1
Atf2	Mm00833804_g1	Atp1b1	Mm00437612_m1
Atf3	Mm00476032_m1	Atp2a2	Mm00437634_m1
Atf4	Mm00515324_m1	Bop	Mm00477663_m1
Bach1	Mm00476077_m1	Cacna1c	Mm00437917_m1
Bcl11a	Mm00479358_m1	Cacna1d	Mm00551384_m1
Bcl6	Mm00477633_m1	Cacna1g	Mm00486549_m1
Bcl6b	Mm00455914_m1	Cacna1h	Mm00445369_m1
Cacna1c	Mm00437917_m1	Cacna2d1	Mm00486607_m1
Cacna1d	Mm00551384_m1	Cacna2d2	Mm00457825_m1
Cacna1g	Mm00486549_m1	Cacna2d3	Mm00486613_m1
Cacna2d1	Mm00486607_m1	Cacn1	Mm00518940_m1
Cacna2d2	Mm00457825_m1	Cacn2	Mm005659092_m1
Cacn3b	Mm00432233_m1	Cacn3	Mm00432233_m1
Ccfa2t1h	Mm00486771_m1	Cacn7	Mm00519216_m1
Cited1	Mm00455934_m1	Calm1	Mm00486655_m1
Cited2	Mm00516211_m1	Calm3	Mm00482929_m1
Cnbp1	Mm00488938_m1	Casq2	Mm00486738_m1
Cops2	Mm00487179_m1	Cd4	Mm00442754_m1
Cops5	Mm00489065_m1	Cfr	Mm00445197_m1
Creb1	Mm00501607_m1	Clcn2	Mm00438245_m1
Creb3	Mm00457268_m1	Clcn3	Mm00432566_m1
Crem	Mm00516346_m1	Cnn1	Mm00487032_m1
Cri1	Mm00517974_s1	Col6a1	Mm00487160_m1
Cutl1	Mm00501628_m1	Dlgh1	Mm00492174_m1
Dazap2	Mm00726901_s1	Dlgh4	Mm00492193_m1
Ddx20	Mm00600300_g1	Eif4g2	Mm00469036_m1
Dmr2	Mm00659912_m1	G6pdx	Mm00656735_g1
E2f1	Mm00432939_m1	Gapd	Mm00486655_m1
E2f2	Mm00624964_m1	Gata4	Mm00484689_m1
E2f4	Mm00514160_m1	Gja1	Mm00439105_m1
E2f5	Mm00468171_m1	Gja4	Mm00433610_s1
E2f6	Mm00519030_m1	Gja5	Mm00433619_s1
E4f1	Mm00468177_m1	Gja7	Mm00433624_m1
Eif4g2	Mm00469036_m1	Hcn1	Mm00468832_m1
En2	Mm00438710_m1	Hcn2	Mm00468538_m1
Ep300	Mm00625535_m1	Hcn3	Mm00468543_m1
Erg	Mm00504897_m1	Hprt	Mm00469668_m1
Esr1	Mm00433149_m1	Hsp96	Mm00658568_gH
Esr2	Mm00516267_m1	Hspa1	Mm00442854_m1
Ets2	Mm00468972_m1	It6	Mm00446190_m1
Etv1	Mm00514804_m1	Itrp2	Mm00444937_m1
Fkhl18	Mm00809617_s1	Kcna1	Mm00439977_s1
Fhl1	Mm00484410_m1	Kcna2	Mm00434584_s1
Fos	Mm00487425_m1	Kcna4	Mm00445241_s1
Foxa3	Mm00484714_m1	Kcna5	Mm00524346_s1
Foxc2	Mm00546194_s1	Kcna6	Mm00496625_s1
Foxk1	Mm00440301_m1	Kcnab1	Mm00440018_m1
Foxm1	Mm00514924_m1	Kcnab2	Mm00440022_m1
Foxo1	Mm00490672_m1	Kcnb1	Mm00492791_m1
Fus	Mm00836363_g1	Kcnd1	Mm00492796_m1
Gabpa	Mm00484598_m1	Kcnd2	Mm00498065_m1
Gapdh	Mm00999915_g1	Kcnd3	Mm00498260_m1
Gata1	Mm00484678_m1	Kcne1	Mm00434615_m1
Gata3	Mm00484683_m1	Kcne11	Mm00517596_s1
Gata4	Mm00484689_m1	Kcne2	Mm00506492_m1
Gata5	Mm00484692_m1	Kcne3	Mm00445119_m1
Gata6	Mm00802636_m1	Kcnh2	Mm00465370_m1
Gja1	Mm00439105_m1	Kcnip1	Mm00471928_m1
Gja5	Mm00433619_s1	Kcnip2	Mm00518914_m1
Gja7	Mm00433624_m1	Kcnj11	Mm00440050_s1
Gtf2ird1	Mm00465654_m1	Kcnj12	Mm00440058_s1
Hand1	Mm00433931_m1	Kcnj2	Mm00434616_m1
Hand2	Mm00439247_m1	Kcnj3	Mm00434618_m1
Hcn2	Mm00468538_m1	Kcnj8	Mm00434620_m1
Hes1	Mm00468601_m1	Kcnk2	Mm00440072_m1
Hey1	Mm00468865_m1	Kcnn1	Mm00446259_m1
Hey2	Mm00469280_m1	Kcnn2	Mm00446514_m1
Heyl	Mm00516555_m1	Kcnp1	Mm00434641_m1
Hif1a	Mm00468869_m1	Myh7	Mm00600555_m1
Hix	Mm00468656_m1	Myia	Mm00440378_m1
Hoxa13	Mm00433967_m1	Mylic2a	Mm00491655_m1
Hoxa9	Mm00439364_m1	Myipc	Mm00440384_m1
Hprt	Mm00469668_m1	Nkx2-5	Mm00657783_m1
Hsf1	Mm00801771_g1	Nppb	Mm00435304_g1
Htatip	Mm00724374_m1	Pias3	Mm00450739_m1
Irx3	Mm00500463_m1	Pln	Mm00452263_m1
Irx4	Mm00502170_m1	Pou5f1	Mm00658129_gH
Irx5	Mm00502107_m1	Prkaca	Mm00660092_m1
Isgf3g	Mm00492679_m1	Prkce	Mm00440894_m1
Jun	Mm00495062_s1	Ryr2	Mm00465877_m1
Jund1	Mm00495088_s1	Scn1b	Mm00441210_m1
Jund2	Mm00473044_m1	Scn3a	Mm00658167_m1
Klf13	Mm00727486_s1	Scn3b	Mm00463369_m1
Klf15	Mm00517792_m1	Scn4a	Mm00500103_m1
Klf16	Mm00652334_m1	Scn5a	Mm00451971_m1
Klf2	Mm00500486_g1	Slc8a1	Mm00441524_m1
Mafk	Mm00456782_m1	Tgfb1	Mm00441724_m1
Polr2a	Mm00839493_m1	Tnni3	Mm00437164_m1
Scn1b	Mm00441210_m1	Tnnt2	Mm00441922_m1
Scn3b	Mm00463369_m1	Uchl1	Mm00495900_m1
Scn5a	Mm00451971_m1	Ywhae	Mm00494246_m1

Human TLDA	
ABCC8	Hs01093761_m1
ABCC9	Hs00245832_m1
ATP1A3	Hs00958036_m1
ATP1B1	Hs00426868_g1
ATP2A2	Hs00544877_m1
ATP2A3	Hs00193090_m1
ATP2B4	Hs00608066_m1
CACNA1C	Hs0167681_m1
CACNA1D	Hs0167753_m1
CACNA1G	Hs00367969_m1
18S	Hs99999901_s1
CACNA1H	Hs01103527_m1
CACNA2D1	Hs00984856_m1
CACNA2D2	Hs01021049_m1
CACNB2	Hs01100744_m1
CALM1	Hs00300085_s1
CALM3	Hs00968732_g1
CASQ2	Hs00154286_m1
GJA1	Hs00748445_s1
GJA5	Hs00270952_s1
GJC1	Hs00271416_s1
GJD3	Hs00987388_s1
HCN1	Hs01085412_m1
HCN2	Hs00606903_m1
HCN3	Hs00380018_m1
HCN4	Hs00975492_m1
ITPR1	Hs00181881_m1
ITPR3	Hs00609908_m1
KCNA2	Hs00270656_m1
KCNA4	Hs00937357_s1
KCNA5	Hs00969279_s1
KCNA7	Hs00361015_m1
KCNAB2	Hs00186308_m1
KCNAB3	Hs01085073_m1
KCNB1	Hs00270657_m1
KCNK4	Hs00428198_m1
KCND2	Hs01054873_m1
KCND3	Hs00542597_m1
KCNE1	Hs00264799_s1
KCNE1L	Hs01085745_s1
KCNE2	Hs00270822_m1
KCNE3	Hs01921543_s1
KCNE4	Hs01851577_s1
KCNH2	Hs04234270_g1
KCNIP2	Hs01552688_g1
KCNJ11	Hs00265026_s1
KCNJ2	Hs01876357_s1
KCNJ3	Hs04334861_s1
KCNJ4	Hs00705379_s1
KCNJ5	Hs00168476_m1
KCNJ8	Hs00958961_m1
KCNK1	Hs00158428_m1
KCNK3	Hs00605529_m1
KCNK5	Hs00186652_m1
KCNQ1	Hs00923522_m1
NPPA	Hs00383230_g1
NPPB	Hs01057466_g1
PLN	Hs01848144_s1
PPP3CA	Hs00174223_m1
RYR2	Hs00181461_m1
SCN10A	Hs01045137_m1
SCN1B	Hs03987893_m1
SCN2B	Hs00394952_m1
SCN3A	Hs00366913_m1
SCN3B	Hs01024483_m1
SCN4A	Hs01109480_m1
SCN4B	Hs03681025_m1
SCN5A	Hs00165693_m1
SCN7A	Hs00161546_m1
SCN9A	Hs00161567_m1
SLC8A1	Hs01062258_m1
ANK2	Hs00153998_m1
ACTB	Hs99999903_m1
RPL13A	Hs04194366_g1
GATA3	Hs00231122_m1
GATA4	Hs00171403_m1
GATA5	Hs00388359_m1
GATA6	Hs00232018_m1
HEY2	Hs00232622_m1
IRX3	Hs01124217_g1
IRX4	Hs00212560_m1
IRX5	Hs04334749_m1
TBX2	Hs00911929_m1
TBX3	Hs00195612_m1
TBX5	Hs00361155_m1
NKX2-5	Hs00231763_m1
TNNI3	Hs00165957_m1
TNNI2	Hs00943911_m1
MYH6	Hs01101425_m1
MYH7	Hs01110632_g1
RRAD	Hs00188163_m1
CLASP2	Hs00380556_m1
GPD1L	Hs00380518_m1
B2M	Hs00187842_m1
MYL7	Hs01085998_g1
MYL2	Hs00166405_m1

Supplemental Table 3. Primers used to amplify DNA after ChIP for IRX5.

	Primer sequences	Position relative to TSS
IRX5- <i>SCN5A</i> -BS1	Fw: tacctgcacaccattctccc Rv: agagggtcagggtgagagat	-7611 -7527
IRX5- <i>SCN5A</i> -BS2	Fw: ttctctgccctcctctctct Rv: cgccaccaagacgatcaaa	+847 +929
IRX5- <i>SCN5A</i> -BS3	Fw: ttgatcgtctttggtggcg Rv: atcctgatctggctgtgctc	+929 +1112
IRX5- <i>GJA5</i> -CP	Fw: agcccctccttcattcactc Rv: ctgtctgtgttctcccagga	-55 +48
IRX5- <i>GJA1</i> -BS1	Fw: ctctttcagcaggtcagtcc Rv: gacaaggaagaggaggctgt	-3272 -3186
IRX5- <i>GJA1</i> -BS2	Fw: tctctctcccattccacca Rv: agaggtaggtgtgagtgacc	-490 -412
GATA4- <i>SCN5A</i> -BSa	Fw: ccgctatgtctgtctgtcc Rv: gcacactcccacactgacc	-268 -201
GATA4- <i>SCN5A</i> -BSb	Fw: cccttccttccttctt Rv: ggtatccgggtcccaatcc	+416 +529
Intergenic region	Fw: agcaccatgataagaaagcca Rv: acccaacagaaatgaaagcct	

TSS: Transcription Start Site; Fw: Forward; Rv: Reverse.

Supplemental Table 4. Solutions used for patch clamp recordings (mM).

	Solution AP		Solution I _{Na}		Solution I _{Ca,L}		AP clamp I _{Na}	
	Intra-pipette	Extra-cellular	Intra-pipette	Extra-cellular	Intra-pipette	Extra-cellular	Intra-pipette	Extra-cellular
Kgluconate	125							
NaCl	5	140	3	20	5		3	130
KCl	20	4						
Hepes	5	10	5	10	10	10	5	10
Glucose		10						
MgCl₂		0.5	2	1.2		1	2	1
CaCl₂		1			2	5		
CsCl			133	110	145		133	10
EGTA			10		5		10	
TEACL			2			160	2	
Na₂ATP			2				2	
CoCl₂				1.8				1.8
Mannitol				30		20		30
MgATP					5			
TTX						0.03		

Supplemental Table 5. Sodium current V50, voltage of halfmaximum activation and inactivation, and K, slope factor. Data are presented as mean \pm SD.

			Ctrl	A150P	N166K
I_{Na}	Activation	V50	-31.51 (\pm 0.21)	-32.19 (\pm 0.32)	-31.09 (\pm 0.34)
		K	6.452 (\pm 0.17)	6.526 (\pm 0.25)	6.736 (\pm 0.26)
	Inactivation	V50	-87.27 (\pm 0.21)	-87.37 (\pm 0.23)	-86.36 (\pm 0.25)
		K	-5.674 (\pm 0.18)	-5.774 (\pm 0.20)	-5.508 (\pm 0.21)